Astron. Astrophys. 256, 56–78 (1992)

ASTRONOMY AND ASTROPHYSICS

Compact Steep-Spectrum 3 CR sources: VLA observations at 1.5, 15 and 22.5 GHz

W.J.M. van Breugel[1], C. Fanti[2,3], R. Fanti[2,3], C. Stanghellini[2,3], R.T. Schilizzi[4], and R.E. Spencer[5]

[1] Institute of Geophysics and Planetary Physics, Lawrence Livermore National Laboratory, P.O. Box 808, L-413, Livermore, CA 94550, USA
[2] Dipartimento di Astronomia, Via Zamboni 33, I-40126, Bologna Italy
[3] Istituto di Radioastronomia del CNR, Via Irnerio 46, I-40126 Bologna, Italy
[4] Netherlands Foundation for Research in Astronomy Radiosterrenwacht Dwingeloo, Postbus 2, NL-7990 AA, The Netherlands
[5] Nuffield Radio Astronomy Laboratories University of Manchester, Jodrell Bank Macclesfield, Cheshire, SK11 9L, UK

Received July 18, accepted September 4, 1991

Abstract. We present observations of a sample of Compact Steep-Spectrum Sources (CSS) from the 3 CR catalogue, made with the Very Large Array at the frequencies of 1.5, 15 and 22.5 GHz, and with angular resolutions ranging from 0.08 to 4 arcsec. We also present 8.4 GHz observations of 3C 286 and 3C 305.1. Large-scale structure has only been detected in the vicinity of 3C 216, 3C 299, 3C 346 and 3C 380. The low resolution 1.5 GHz data allow stringent upper limits to be set to any large scale (tens of kiloparsecs) low brightness emission in the remaining sources. The observations at the higher frequencies provide maps with the best resolution which can be achieved with the VLA (0.08–0.15 arcsec), and give additional spectral and polarization information.

Key words: radio continuum: galaxies – quasars: general – galaxies: jets – techniques: interferometric

1. Introduction

Over the past several years we have been studying a representative sample of Compact Steep-Spectrum Sources (CSS) at several wavelengths and resolutions using the European VLBI Network, and the MERLIN and VLA interferometers. References to our own observing program (see Table 1) and to previous results can be found in Fanti et al. (1990). There further references to the literature and a discussion of the general properties of CSSs are also given.

In this paper we present the results of observations of 26 CSSs from the 3 CR catalogue, carried out with the VLA at several frequencies. Our source list with various relevant parameters is given in Table 2.

The aims of our observations were twofold:

(1) To establish whether CSSs have low-brightness emission components extending over scales of several tens of kiloparsecs, by means of observations with moderate resolution but high surface brightness sensitivity. This search was motivated by the existence of objects like 3C 236 (Schilizzi et al. 1988) and 3C 293 (Bridle et al. 1981) which are characterized by a dominant steep-spectrum, kiloparsec-sized central component (steep spectrum core: SSC) plus a double-lobed low brightness structure. The low-brightness structures in 3C 236 and 3C 293 contain 53% and 30%, respectively, of the total luminosities of their steep spectrum cores, at the frequency of 1.4 GHz. Since the radio structures of the cores in 3C 236 and 3C 293 are similar to those seen in CSS sources, we decided to investigate whether extended emission is also present around most of the CSSs. The data available in the literature provided limits to extended structure of $\sim$10–20% of the luminosity of the compact components, so that further observations were needed.

(2) To obtain structural information at high frequencies with angular resolutions comparable to those achievable around 1.5 GHz with MERLIN and VLBI. The principal goal was to search for the cores of the CSSs. The 15 GHz observations complete the sub-sample of CSSs from the 3 CR catalogue, which was begun by van Breugel et al. (1984, vBMH).

Some of the brightest sources were observed at 22.5 GHz, yielding the highest possible resolution maps obtainable at the VLA ($\sim$0.″08). Three sources (3C 286, 3C 299, and 3C 305.1) were also observed at 8.4 GHz, presently the most sensitive high frequency system available at the VLA. Two of them (3C 286 and 3C 305.1) are presented here; 3C 299 will be discussed in a separate paper together with detailed optical observations.

2. Observations and data reduction

2.1. 1.5 GHz

The observations were made in September and November 1987 with the VLA, in the A- and B-configurations, at frequencies of 1465 and 1515 MHz, with a bandwidth of 50 MHz. Typical observations lasted from 10 to 30 min, depending on source intensity and observing schedule constraints.

The data for the two frequencies were reduced independently with the NRAO AIPS image processing package, following standard procedures. The peak and total flux densities of the sources at the two frequencies differed by 2–3%, as expected from their steep power-law spectra.

Send offprint requests to: R. Fanti (Istituto di Radioastronomia)

Table 1. Observational status of the 3 CR CSS sample

Array	ν (GHz)	Reference
VLA	1.5	Present paper
	5.0	van Breugel et al. 1984; Spencer et al. 1989
	15.0	van Breugel et al. 1984; present paper; Spencer et al. 1989
	22.5	Present paper
Merlin	1.6	Spencer et al. 1989
	5.0	Akujor et al. 1991a
VLBI	0.6	Nan Rendong et al. 1991
	1.6	Fanti et al. 1985; Spencer et al. 1991 and references therein
	5.0	Fanti et al. 1986, 1989

Table 2. Compact Steep-Spectrum Sources from the 3 CR catalogue

Name	z	Id(m_v)	Name	z	Id(m_v)
3C 43 0127+23	1.46	Q(20.0)	3C 286 1328+30	0.85	Q(17.3)
3C 48 0134+32	0.37	Q(16.2)	3C 287 1328+27	1.06	Q(17.7)
3C 49 0138+13	0.62	G(22.0)	3C 298 1416+06	1.44	Q(16.8)
3C 67 0221+27	0.31	G(18.0)	3C 299 1419+41	0.37	Q(19.5)
3C 119 0429+41	0.41	Q(20.0)	3C 303.1 1443+77	0.27	G(19.0)
3C 138 0518+16	0.76	Q(17.9)	3C 305.1 1447+77	1.13	G(21.0)
3C 147 0538+49	0.55	Q(16.9)	3C 309.1 1458+71	0.9	Q(16.8)
3C 186 0740+38	1.06	Q(17.6)	3C 318 1517+20	0.75	G(20.3)
3C 190 0758+14	1.2	Q(20.0)	3C 343 1634+62	0.99	Q(20.6)
3C 216 0908+43	0.67	Q(18.5)	3C 343.1 1637+62	0.75	G(20.8)
3C 237 1005+07	0.88	G(21)	3C 346 1641+17	0.16	G(17.2)
3C 241 1019+22	1.62	G(>22)	3C 380 1828+48	0.69	Q(16.8)
3C 268.3 1203+64	0.37	G(19.0)	3C 454 2249+18	1.76	Q(18.5)

Notes: Redshift (z), optical identification (Id) and magnitudes (m_v) are from Spinrad et al. (1985)

Maps were produced with size of 1024 × 1024 points for the B-configuration, corresponding to a total angular size of ~17′ × 17′. Typically two to three iterations of self-calibration were applied to the data before obtaining a satisfactory map of the source. In a limited number of cases the quality of the map was affected by sidelobes of confusing strong sources outside of the synthesized map. In this case the confusing sources were located and subtracted from the visibilities.

The A-configuration maps were generally 256 × 256 points (~75″ × 75″), except in those cases where the B-configuration map had shown distant confusing sources.

The maps obtained at this frequency have a typical *dynamic range* (defined as the ratio between the brightness peak and the *rms noise* computed at more than 5 beams from the field center) of 5000 : 1. Closer to the source the *rms noise* is ~2 times worse. The resolution is ~1″.5 and ~4″ for the A- and for the B-configuration data, respectively.

2.2. 15 GHz

The 15 GHz observations were made using the VLA in the A-configuration in September 1984 using a frequency of 14965 MHz and a bandwidth of 50 MHz. Observing times were 30–45 min, divided over 2–3 scans at different hour angles to obtain better u–v coverage.

Standard calibration and reduction techniques were used, allowing also polarization maps to be made, as described for previous 15 GHz VLA observations of CSSs by vBMH. In particular, self-calibration techniques were essential to achieve low noise levels and good dynamic range. Occasionally a point source model, using source positions available in the literature, was needed for the first iteration of the self-calibration procedure.

The uncertainties in the absolute positions are estimated to be 0.2″. Typical values for the rms noise are 0.5 mJy beam^{-1}. The angular resolution of the maps is ~0.15″.

2.3. 22.5 GHz

Interspersed with the 15 GHz observations we also observed some of the strongest CSSs at 22485 MHz. Observing time, calibration and data analysis were similar to that of the 15 GHz observations. However, the 22.5 GHz data were of considerably lower quality due to less sensitive receivers and the significant corruption of the phases due to atmospheric fluctuations. Self-calibration using point source models from the 15 GHz data was necessary in virtually all cases during the first iteration. No correction was made for atmospheric extinction, which can be significant at low elevations (Spangler 1982), so that the flux density scale is uncertain by as much as 15%.

Typical values for the rms noise is ~2.5 mJy beam area^{-1}. The angular resolution of the maps is ~80 m arcsec. Absolute position uncertainties are sometimes worse than those of the 15 GHz observations. No polarization calibration was attempted.

2.4. 8.4 GHz

The superior sensitivity of the 8.4 GHz receivers at the VLA makes this the frequency of choice when searching for faint radio cores in CSS sources. This was well demonstrated by the detection of the core in 3C 299. A detailed radio and optical study of

Table 3. VLA data at 1.5, 15 and 22.5 GHz

Name	1.5 GHz			15 GHz			22.5 GHz		
	Flux (mJy)	Noise (mJy beam^{-1})	Size (arcsec)	Flux (mJy)	Noise (mJy beam^{-1})	Size (arcsec)	Flux (mJy)	Noise (mJy beam^{-1})	Size (arcsec)
3C 43 0127+23	2857	0.35	2.4	453	0.76	(a)[b]			
3C 48 0134+32	15843	2.0	0.22	2754	2.7 vBMH	0.4	1422	2.7	0.38
3C 49 0138+13	2630	0.4	0.91	284	0.5	1.1			
3C 67 0221+27	2935	0.55	2.1	252	0.53	2.5	51	3.3	<0.05[b]
3C 119 0429+41	8545	1.2	0.10	1685	3.1 vBMH	<0.05	1110	3.4	0.05
3C 138 0518+16	8314	0.9	0.28	2616	2.5 vBMH	0.65	1307	5.3	0.43[b]
3C 147 0538+49	21165	2.9	0.46	3470	2.0 vBMH	0.7	1750	2.2	0.62
3C 186 0740+38	1130	0.26	1.8	42	— CSMM	1.6			
3C 190 0758+14	2470	0.35	3.1	171	0.64	2.7			
3C 216 0908+43	3745	0.45	~9	1035	1.5	(a)[b]			
3C 237 1005+07	6180	1.0	1.3	369	0.45	1.4			
3C 241 1019+22	1600	0.3	0.9	61	0.32	0.84			
3C 268.3 1203+64	3610	0.6	1.45	>281	3.5 vBMH	0.86			
3C 286 1328+30	14450	2.5	2.6	4201	3.4 vBMH	<0.05[b]	2695	4.0	0.04[b]
3C 287 1328+25	6760	1.0	0.14	1875	2.8 vBMH	0.06	1110	2.2	0.05
3C 298 1416+06	5680	1.1	1.6	447	0.7	1.5	316	2.6	1.51
3C 299 1419+41	2700	0.28	11.9	242	1.0	0.8			
3C 303.1 1443+77	1685	0.43	1.8	75	0.4	1.8	47	2.1	0.1[b]
3C 305.1 1447+77	1540	0.46	2.0	90	0.4	2.4			
3C 309.1 1458+71	7230	1.1	1.2	1769	2.0 vBMH	0.94			
3C 318 1517+20	2525	0.24	0.8	226	0.6	0.7	123	2.1	(a)[b]
3C 343 1634+62	4710	0.7	0.3	484	2.6 vBMH	0.05	264	2.4	0.07

Table 3 (continued)

Name	1.5 GHz			15 GHz			22.5 GHz		
	Flux (mJy)	Noise (mJy beam^{-1})	Size (arcsec)	Flux (mJy)	Noise (mJy beam^{-1})	Size (arcsec)	Flux (mJy)	Noise (mJy beam^{-1})	Size (arcsec)
3C 343.1 1637+62	4350	0.9	0.4	342	0.8	0.3	238	2.3	0.27
3C 346 1641+17	3525	0.21	14×12	384	0.46	~4[b]			
3C 380 1828+48	13650	1.7	16×12						
3C 454 2249+18	2035	0.5	0.7	335	— CSMM	~0.8			

Notes: (a) see map; [b] Only a part of the total radio structure has been revealed. vBMH: data from van Breugel et al. (1984); CSMM: data from Cawthorne et al. (1986). Integrated flux densities, rms noise values, and maximum angular sizes derived from the maps. At 1.5 GHz sizes are FWHM from Gaussian fit, at 15 and 22.5 GHz we give the maximum source extent seen in the map. Sizes are deconvolved for beam smearing.

Table 4. Source component parameters at 15 and 22.5 GHz

Name		15 GHz			22.5 GHz	
		Flux (mJy)	Size (mas)	p.a. (o)	Flux (mJy)	Size (mas)
3C 43						
	A	418	See map			
	B	35	See map			
3C 48						
	A				765	140
	B				612	160
3C 49						
	A	242	35×21	(155)		
	B	6	<90			
	C	10	See map			
	D	26	See map			
3C 67						
	A	89	See map			
	B	163	97×62	(167)	51	<50
3C 119					1110	50
3C 138						
	A				385	40
	B				922	See map
3C 147						
	A				500	100
	B				1190	<40
	C				54	See map
3C 190						
	A	50	105×73	(174)		
	B	43	97×44	(46)		
	C	39	<44			
	D	39	79×55	(56)		

Table 4 (continued)

Name		15 GHz			22.5 GHz	
		Flux (mJy)	Size (mas)	p.a. (o)	Flux (mJy)	Size (mas)
3C 216						
	A	910	60 × 30	(146)		
	B	125	See map			
3C 237						
	A	224	160 × 100	(80)		
	B	2.2	< 60			
	C	143	~400 × 300	(90)		
3C 241						
	A1	34	45 × 17	(94)		
	A2	12	43 × 31	(82)		
	B	3.4	< 60			
	C	11	56 × 20	(101)		
3C 286					2695	40
3C 287					1110	50
3C 298						
	A	50	50 × 45	(158)	34	90
	B1	210	< 50		174	< 30
	B2	69	< 110		70	160
	C1	32	96 × 65	(97)	35	See map
	C2	85	98 × 68	(29)	60	130
3C 299						
	A	242	~850 × 460	(30)		
3C 303.1						
	A	5	See map			
	B	70	110 × 39	(125)	47	95
3C 305.1						
	A	22	149 × 119	(65)		
	B	5	< 130			
	C	15.5	345 × 153	(25)		
	D	47	89 × 46	(19)		
3C 318						
	A	29	70 × 46	(122)		
	B	197	See map		123	See map
3C 343					264	70
3C 343.1						
	A	230	59 × 23	(113)	163	60
	B	112	< 80		81	< 80
3C 346						
	A	243	< 39			
	B	14	186 × 107	(102)		
	C	80	97 × 79	(93)		
	D	8	< 240			
	E	39	See map			

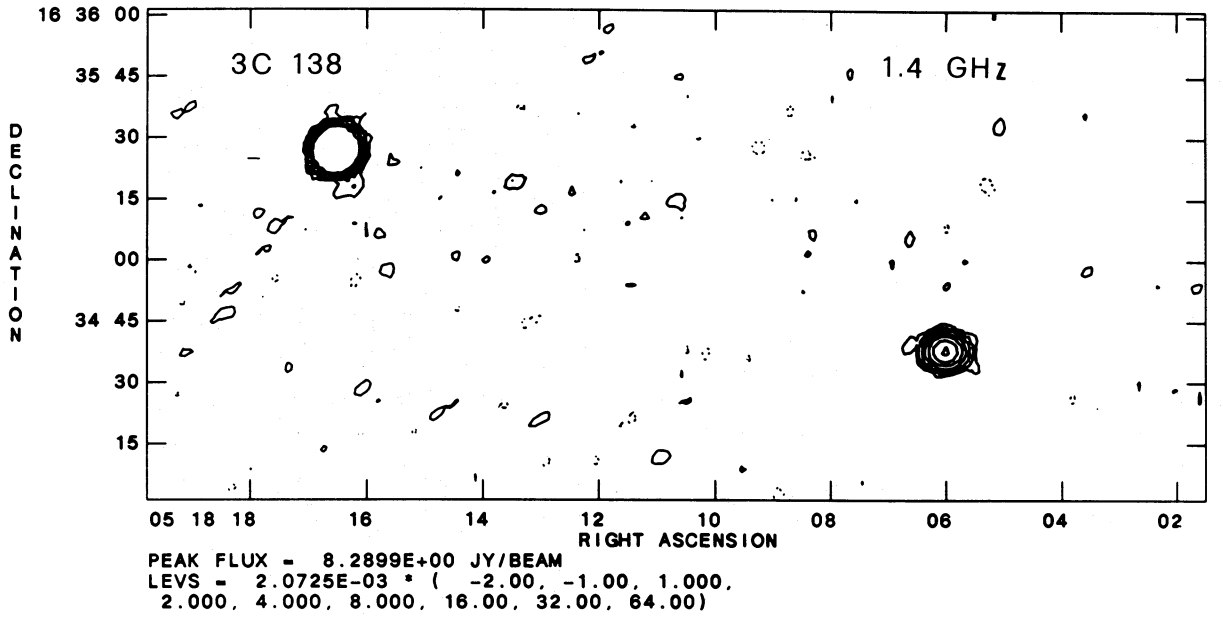

Fig. 1

Figs. 1–6. VLA maps at 1.5 GHz

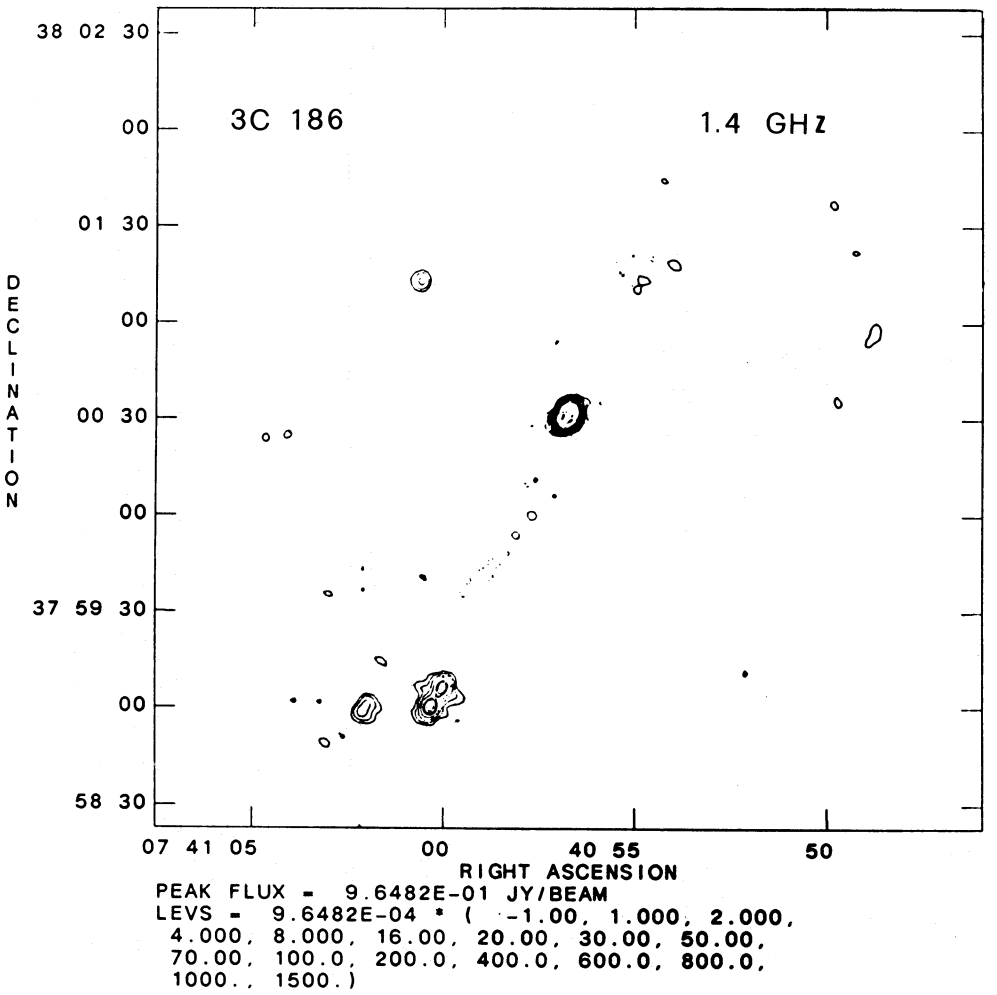

Fig. 2

this source is reported elsewhere (van Breugel et al., in preparation). We observed also two other sources (3C 286 and 3C 305.1) at this frequency, and these are discussed later in the present paper. The angular resolution of the maps is 0.″22.

3. Results

Our results are summarized in Tables 3 and 4. Table 3 gives total source flux density, rms noise level and maximum source extent at the various observing frequencies. At 1.5 GHz the flux density and noise values are from the B-configuration observations. The corresponding numbers for the A-configuration are quite similar. Table 4 gives the parameters of individual components in sources well resolved at 15 and 22.5 GHz. Components are labelled A, B, C, . . . from west to east.

The maps of all the well resolved sources are shown in Figs. 1–6 for 1.5 GHz and in Figs. 7–24 for 15, 22.5 and 8.4 GHz, in right ascension order.

3.1. 1.5 GHz

Most of the sources appear unresolved by the B-configuration or just slightly resolved by the A-configuration, consistent with what was known from previous sub-arcsec observations (MERLIN and VLBI). The only well resolved sources, with sizes >4″, are 3C 216, 3C 346 and 3C 380. 3C 299 has a secondary component 12″ SW from the main component.

In view of the rather different resolving powers, comparison of the flux densities from A- and B-configuration might, in principle, allow recognition of faint emission, not individually detected, from areas of a few arcsec around the CSS component. In practice no significant indication of such extensions has been found on these scales.

Comparison of the flux densities obtained from the two configurations has been therefore used to estimate the internal accuracy of the flux density measurements. They are not systematically different within an rms uncertainty of ~2%. This figure represents the flux calibration uncertainty in our observations.

A further important comparison is between the flux densities measured by MERLIN with 0.″3 resolution (Spencer et al. 1989) and our VLA data. This comparison could reveal emission on arcsec or sub-arcsec scales resolved by MERLIN but contributing to the VLA flux density. This comparison does not show any significant systematic difference within a standard deviation of ~130 mJy, which is expected to arise from uncertainties in the respective flux calibrations.

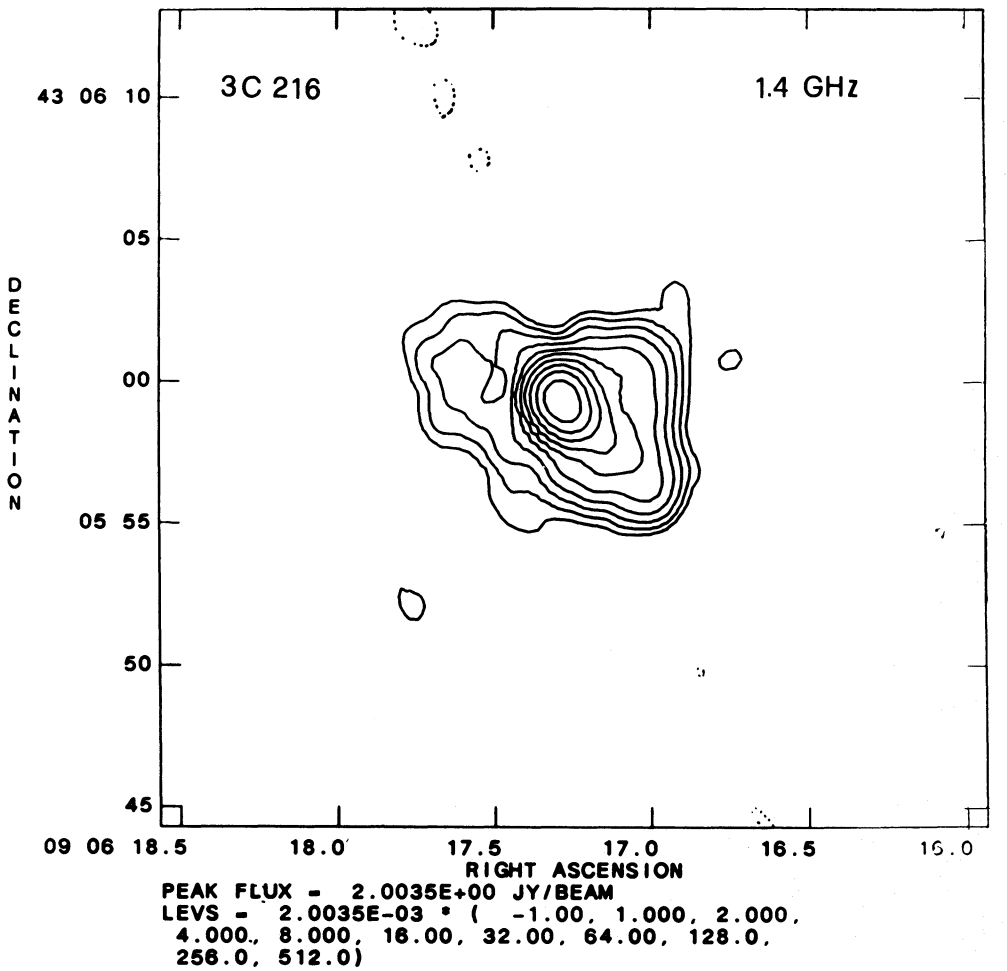

Fig. 3

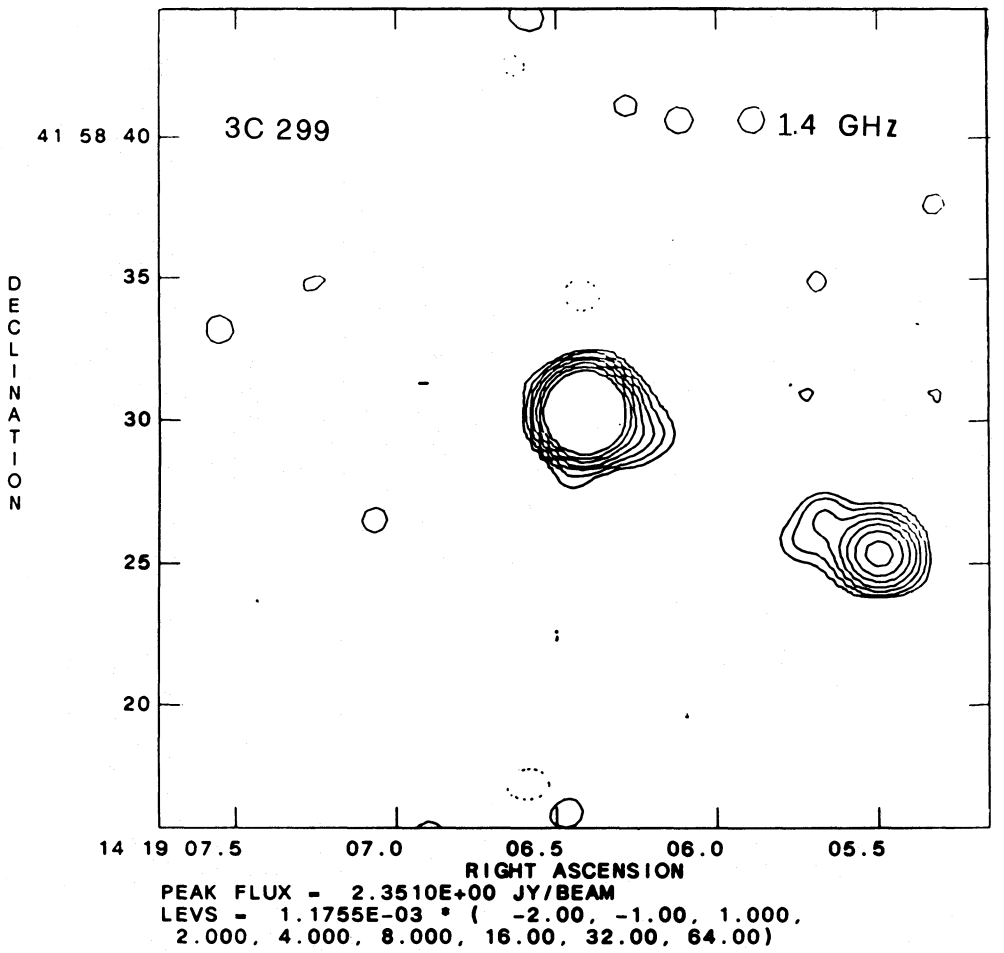

Fig. 4

3.2. 15 GHz

Most sources are well resolved at this frequency. For only four of them (3C 119, 3C 286, 3C 287, 3C 343) the angular resolution is not adequate to map the radio structure. See references in Fanti et al. (1990) for higher resolution VLBI observations. Total flux densities of individual components (Table 4) were derived using Gaussian model fits or, for well resolved components, by integrating over the appropriate regions in the maps. The total flux densities of each of the sources, as determined from the maps, were compared with plots of the visibility amplitudes as well as with single dish measurements from Kuhr et al. (1981). Notes on whether much radio structure may have remained undetected in our VLA maps are included in our comments on the individual sources.

3.3. 22.5 GHz

The 22.5 GHz maps are primarily of interest because of the higher resolution provided ($\sim$0.″08). They are useful for determining relative strength of compact components which may help locating the radio cores in CSSs.

3.4. 8.4 GHz

Here we show the maps of the CSSs 3C 286 and 3C 305.1, which were observed for a total time of 15 and 30 min, respectively. The map for 3C 286 is dynamic range limited at a peak/(rms noise) ratio of 3700:1. The map for 3C 305.1 is noise limited at an rms level of 44 μJy beam^{-1}.

4. Discussion

4.1. Extended emission around CSSs?

In only four cases is extended emission clearly detected on scales of several arcsecs around the compact component: these are 3C 216, 3C 299, 3C 346 and 3C 380. These sources were already known to have such extended emission (Barthel et al. 1988; vBMH; Stannard private communication; Pearson et al. 1985) and our results are fully consistent with the earlier work. For each of the four sources the extended emission is $\sim$24%, 5%, 60%, 50% respectively of the total luminosity.

3C 299 is now clearly a very asymmetric double (see Sect. 5). The other three sources (3C 216, 3C 346 and 3C 380) differ from 3C 236 and 3C 293 in that: a) they have bright radio cores and

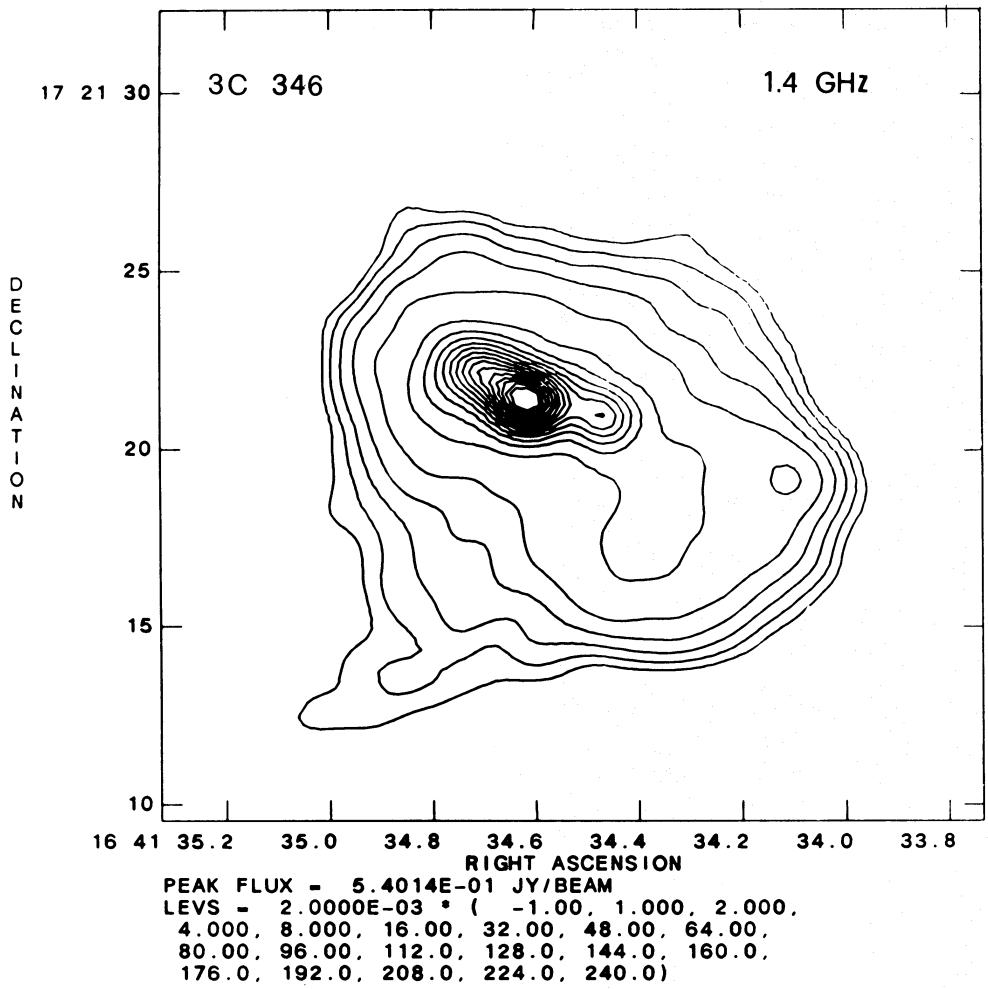

Fig. 5

bright one-sided jets; and b) their extended emission has an ellipsoidal *halo* shape and rather uniform surface brightness. In view of these differences we think that the two sets of sources are different in nature. We suggest that 3C 216, 3C 346 and 3C 380 may be large size doubles seen in projection with a relatively small angle with respect to the line of sight. Their relatively bright cores and one-sided jets could then be caused by relativistic Doppler boosting. The extended *halo-like* emission would be due to their radio lobes seen in projection and overlapping with the cores and jets.

The radio sources 3C 236 and 3C 293 do not have such characteristics so that it is unlikely that their CSS central components are caused by projection effects.

For the remaining sources our data allow stringent limits to be set to any large-scale structure with angular scales $<40''$, corresponding to linear sizes <120 kpc for $z>0.5$ ($H_0=100$). On the basis of the dynamic ranges achieved ($\sim 5000/1$) and assuming a conservative limit of $3\times$(rms noise level) for the surface brightness of any undetected extended emission, we can set upper limits to the radio luminosity of extended emission after assuming a value for their sizes. For an extended structure with an overall linear size of 120 kpc, elliptical lobes with axial ratios of 2/3 and major axis of 60 kpc, our limits on brightness sensitivity translate into an upper limit on the monochromatic luminosity of extended emission of $\lesssim 3\%$ of the compact component luminosity (or typically $\lesssim 10^{25.5}$ W/Hz).

A search has also been made for a possible excess, above the expected background, of small size sources around the CSSs. These could be, for example, hot spots of undetected large-scale lobes. It is known that virtually all sources with luminosity above 10^{25} W/Hz, radio galaxies or quasars, exhibit double hot spots with typical brightnesses $\gg 1$ mJy arcsec^{-2}, (e.g. Perley 1989; De Ruiter et al. 1990) which should have been easily detected in our observations. We searched areas with radius of 40″ and 240″ in the A- and B-configuration maps respectively. Source counts at 1.4 GHz by Windhorst (1984) were used to determine the background source level. We do not find any significant excess of point sources in these fields (see Table 6). This supports our result above on the limit for the luminosity of any *extended* lobe. Of course, the possibility remains of extended emission with properties totally different from those of standard lobes of radio galaxies and quasars. In that case our surface brightness limits cannot be easily translated into plausible limits on luminosities.

4.2. Radio cores

The 15 and 22.5 GHz observations resulted in the detection of several weak radio cores which were previously unknown, and

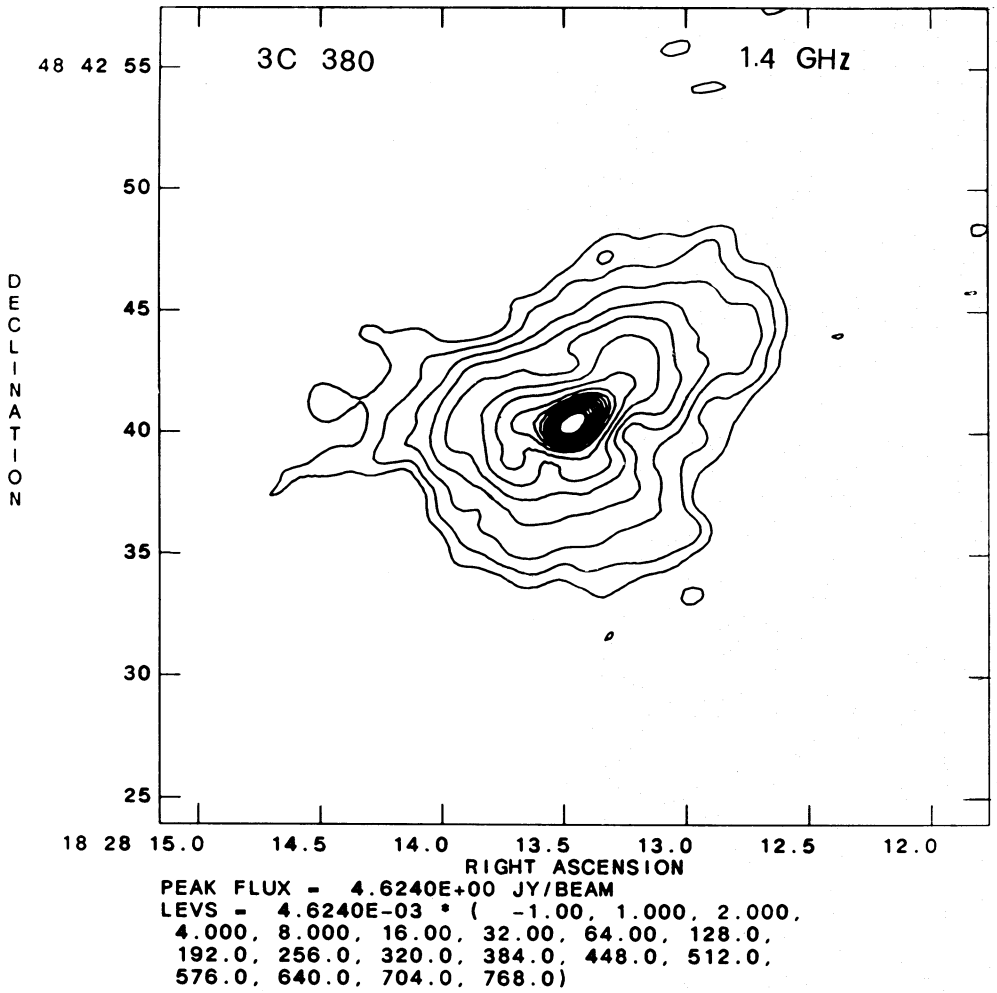

Fig. 6

confirmed a few previous, marginal detections. Their positions are listed in Table 5.

We note that the radio cores of a large number of CSSs remain undetected or uncertain (3C 67, 3C 268.3, 3C 287, 3C 303.1, 3C 305.1, 3C 318, 3C 343, 3C 343.1, 3C 454). Further VLA 8.4 GHz observations of these will be useful. A full discussion of radio cores in 3 CR CSSs is given in Fanti et al. (1990).

4.3. Polarization

Polarization information at 15 GHz, derived from the present observations and from those of vBMH, is now available for the whole 3 CR CSS sample with the exception of 3C 186.

Most sources are significantly polarized. The polarization percentages of individual components are larger at 15 GHz than the average integral value at 5 GHz (vBHM; Saikia et al. 1987). The median value of the polarization percentage in radio components is $\sim(7\pm2)\%$. There is no clear difference between radio lobes and radio jets.

A correlation is found between the position angle of the polarization vector and that of the component extension. About 2/3 of the radio components have a position angle difference larger than 60°. If we assume that the Faraday rotation is negligible at 15 GHz, then this implies that the magnetic field is mostly parallel to the component elongation.

A closer inspection of the polarization maps shows that the magnetic fields in the radio lobes are usually directed along the major axes in their inner regions (3C 67, 3C 237, 3C 298, 3C 305.1) and are tangential in their bright outer parts or hot spots (3C 237, 3C 298, 3C 305.1). This is similar to what is usually found in large-sized doubles. In the jets the magnetic fields can be either parallel or perpendicular, the first case being the more common (see also Spencer et al. 1991).

5. Comments on individual sources

3C 43 (*Fig. 7*): This source has a triple structure (see e.g. Pearson et al. 1985; Spencer et al. 1989, 1991; Akujor et al. 1991b) which is barely resolved in our 1.5 GHz observations. At 15 GHz the northern component is undetected. Components A and B are polarized at this frequency, with percentage polarization ranging from 6–10% for component A to $(50\pm20)\%$ for component B.

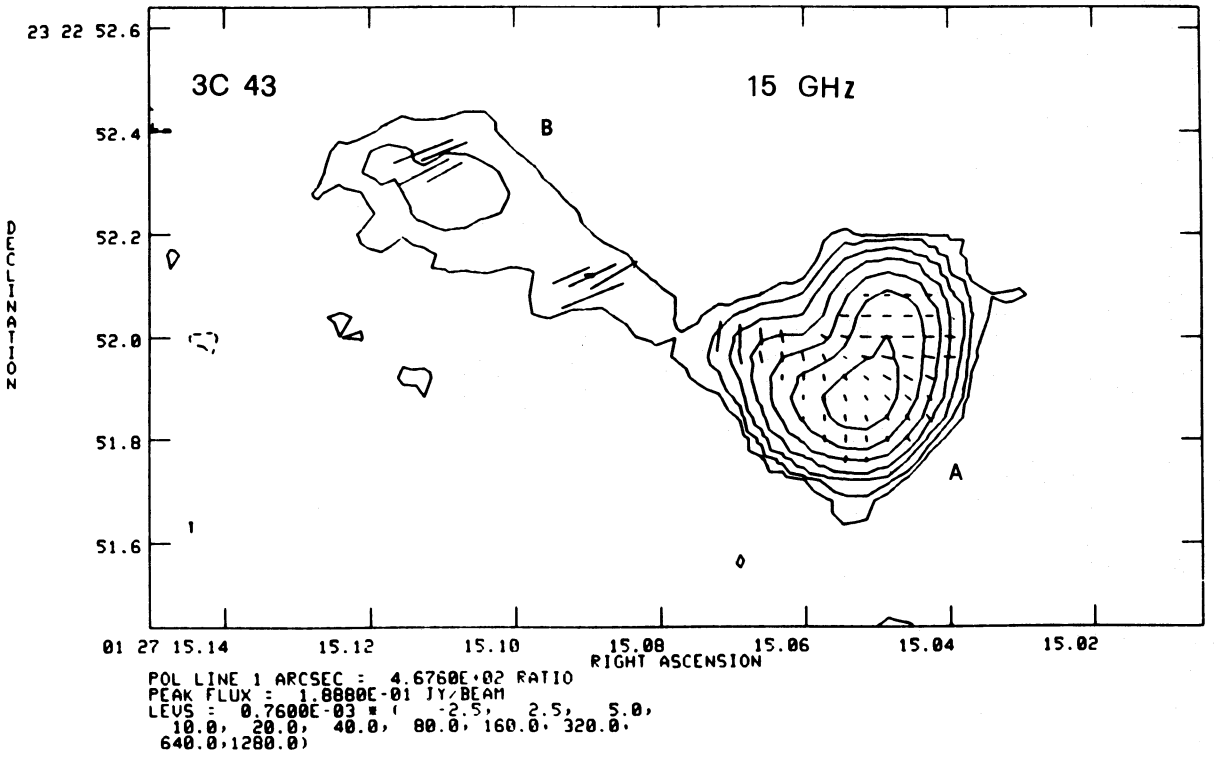

Fig. 7

Figs. 7–24. VLA maps at 15, 22.5 and 8.4 GHz in right ascension order

Table 5. Radio core positions

3C 49	01	38	28.51
	13	38	20.0
3C 190	07	58	45.05
	14	23	04.4
3C 216	09	06	17.26
	43	05	59.0
3C 237	10	05	22.04
	07	44	58.6
3C 241	10	19	09.38
	22	14	39.6
3C 298	14	16	38.77
	06	42	20.9
3C 305.1[a]	14	47	49.35
	77	08	46.7
3C 346	16	41	34.46
	17	21	21.0

[a] Uncertain; see comments to the source

Table 6. Source counts around CSS at 1.5 GHz

Flux range (mJy)	Number of sources[a]	
	Found	Expected
$S > 200$	1	0.3
$200 > S > 80$	2	0.3
$80 > S > 30$	2	1.8
$30 > S > 10$	1	1.1
$10 > S > 3$	2	1.5
Total	8	5.0

[a] In an area of 4′ radius centered on the CSS. The expected value is derived from the source counts of R. Windhorst (Ph.D. thesis)

3C 48 (*Fig. 8*): The 22.5 GHz map, when compared with lower frequency maps of similar resolution (Simon et al. 1990, at 327 MHz; Nan Rendong et al. 1991, at 610 MHz) shows that the southernmost part of component A has a flat or inverted spectrum and is therefore the core, in agreement with Wilkinson et al. 1990.

3C 49 (*Fig. 9*): The compact central component B, undetected at lower frequencies (e.g. Akujor et al. 1991c) is probably the source core (see also Fanti et al. 1989). No polarization is detected at 15 GHz ($<2\%$ and $<10\%$, respectively, for the west and east component).

3C 67 (*Fig. 10*): At 15 GHz component A is polarized $(15 \pm 6)\%$; component B is polarized $(4 \pm 2)\%$. At 22.5 GHz we detect only the southern component, which is unresolved.

3C 138: Two faint sources are found in this field, at 1.5 GHz, at distances of 155″ in p.a. $= -108°$ (Fig. 1) and 243″ in p.a. $= 120°$ from 3C 138 (see also De Waard 1984). There is no evidence in our map for any physical association of these sources with

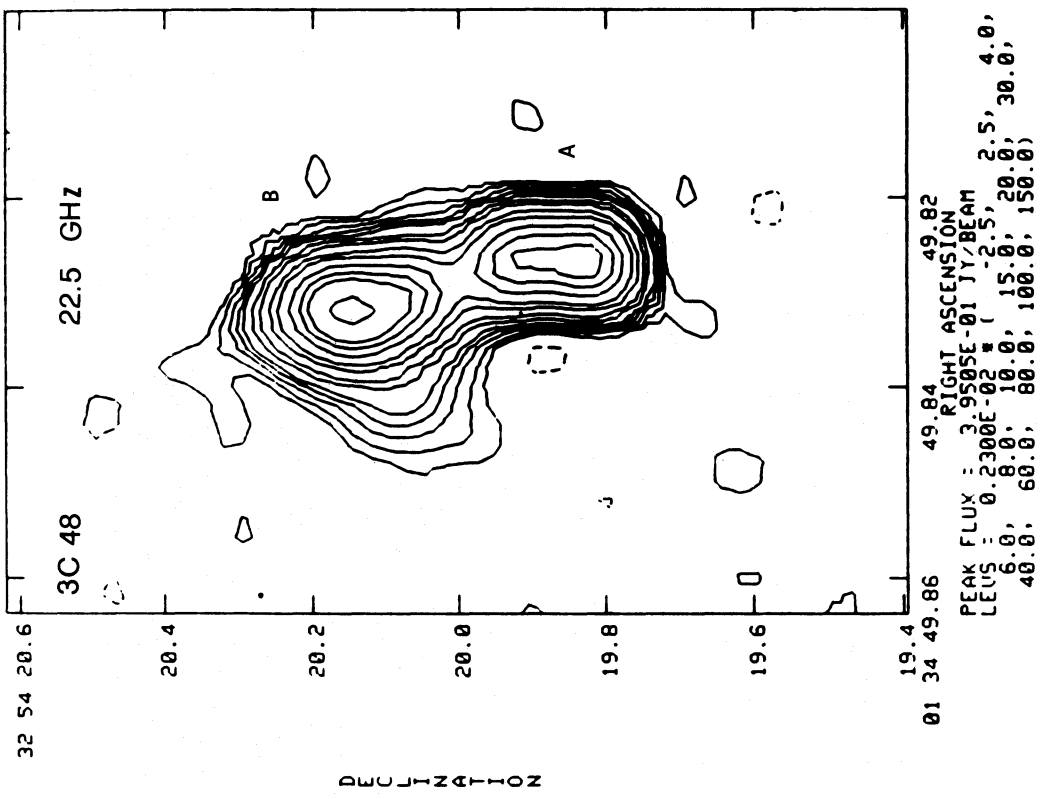

Fig. 8

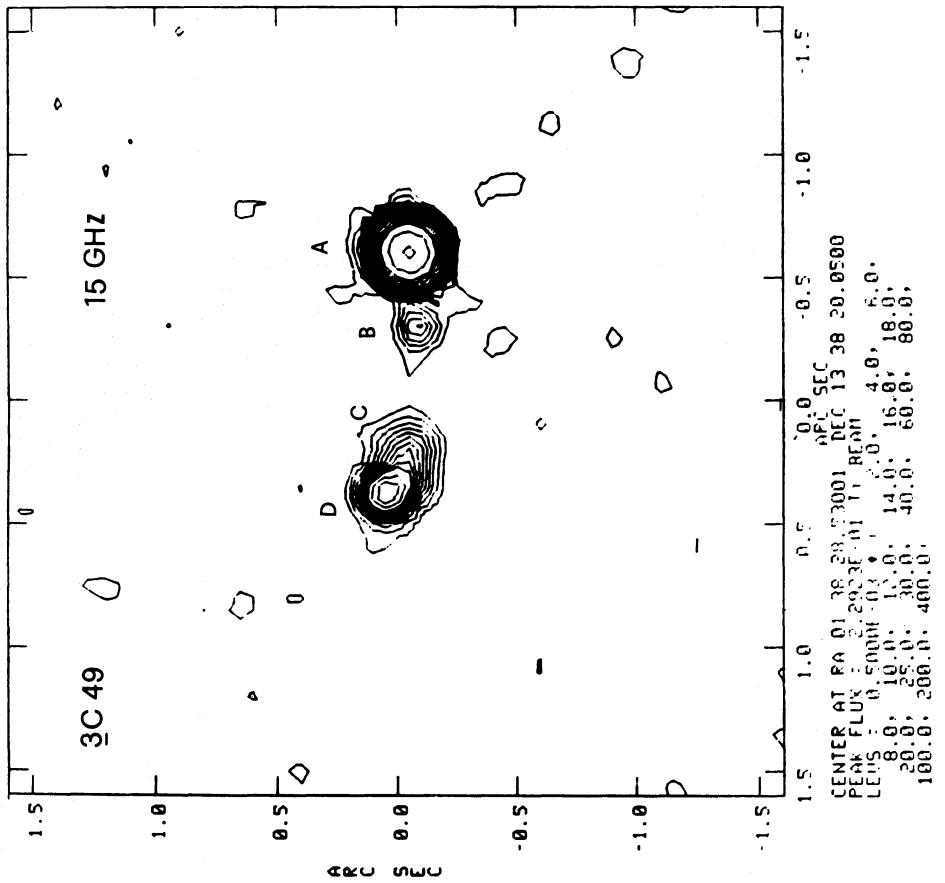

Fig. 9

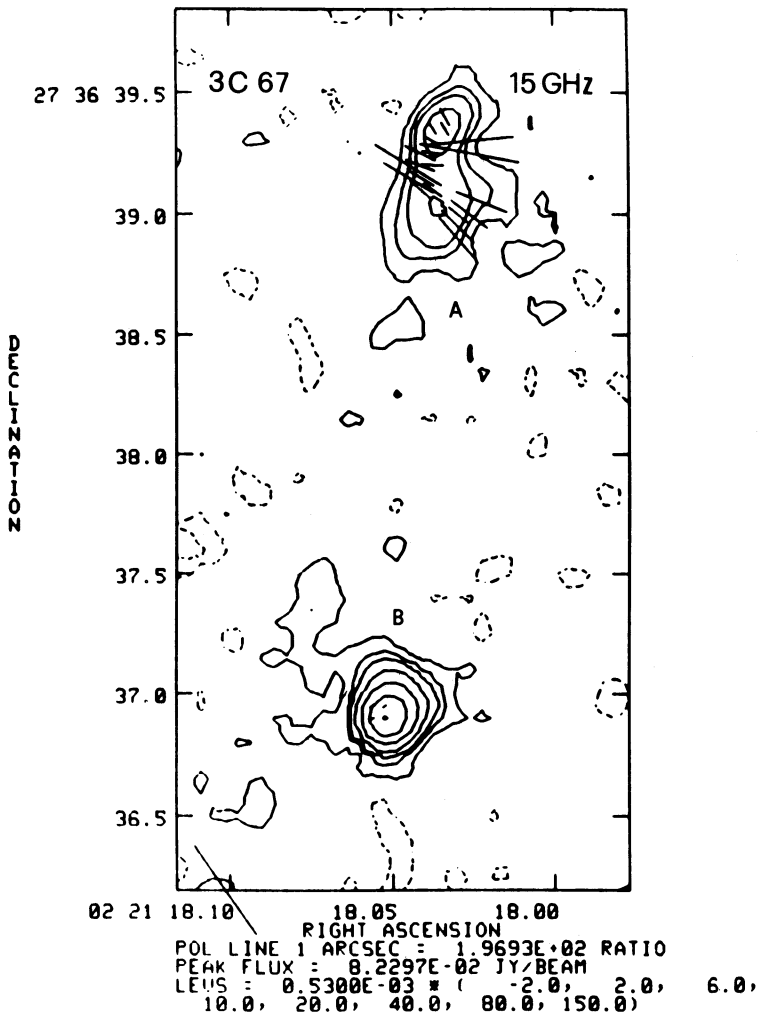

Fig. 10

3C 138. The 22.5 GHz map (Fig. 11) confirms earlier findings (e.g. Fanti et al. 1989) that component A has a flat spectrum and, therefore, contains the radio core.

3C 147 (*Fig. 12*): Akujor et al. (1990), from MERLIN observations at 151 MHz, found a faint halo of $\sim 10''$ around the main component. Our 1.5 GHz data, with a dynamic range of 7000:1 in the B-configuration map, and a similar resolution, do not show any evidence for this halo. The comparison between the A- and B-configuration flux densities also shows no evidence for the halo. A comparison with total power flux measures (quoted in Kuhr et al. 1981) is inconclusive. Therefore the spectrum of any halo component must be very steep.

3C 186: In the field there are three other apparently unrelated sources, one of which is double (Fig. 2). This double plus the other nearby source were noted earlier by Riley and Pooley (1975) and (Schilizzi et al. 1982). A VLA map at 15 GHz has been presented by Cawthorne et al. (1986). A comparison of it with the 50 cm VLBI map by Nan Rendong et al. (1991) shows 3C 186 to have a central core self-absorbed at frequencies below ~ 1 GHz. A prominent jet (Spencer et al. 1991) leads to the N component.

3C 190 (*Fig. 13*): About 130 mJy are missing in our 15 GHz map. This is almost certainly due to a diffuse lobe which is seen in lower frequencies maps (see e.g. Pearson et al. 1985; Spencer et al. 1991), but which is resolved out in our observations. Component A is polarized $(7 \pm 3)\%$ at its southern edge, component B $(10 \pm 2)\%$, component C $< 4\%$, component D $< 4\%$. Component C is the source core (Nan Rendong et al. 1991).

3C 216: At 1.5 GHz (Fig. 3) this source exhibits a low brightness halo consistent with the map of Barthel et al. (1988). This halo accounts for 24% of the total flux density. The bright component has actually a triple structure (Pearson et al. 1985), of which our 15 GHz map (Fig. 14) shows only the central and the northern component (about 100 mJy are missing in our map). Component A is $< 2\%$ polarized at the peak, has a flat spectrum ($\alpha \sim -0.1$, $S \propto \nu^{-\alpha}$) and is therefore believed to be the radio core. Its southern extension is 12% polarized. Component B is 12–20% ($\pm 3\%$) polarized.

3C 237 (*Fig. 15*): In our 15 GHz map ~ 190 mJy are missing. Component A is polarized $(4 \pm 2)\%$; component C is $< 2\%$ polarized at the peak and ranges from 12 to 20% ($\pm 3\%$) in the

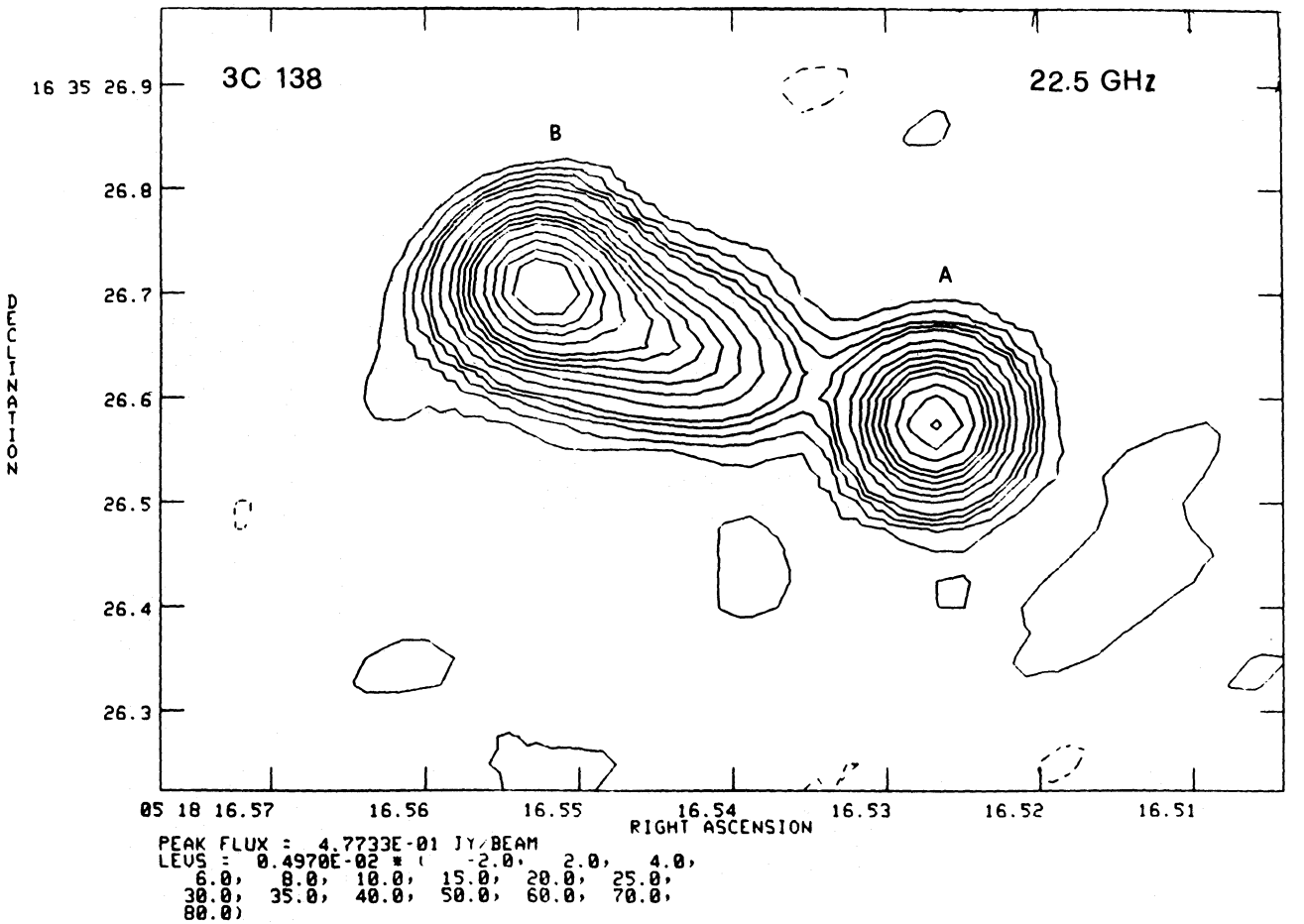

Fig. 11

inner tail. Comparison with the 1.7 GHz data by Fanti et al. (1985) indicates that component B is likely to be the source core.

3C 241 (*Fig. 16*): The source is not polarized (<5–12% in the west component and <15% in eastern one). Comparison with the 1.7 GHz (Fanti et al. 1985) and 5 GHz data (Akujor et al. 1991) indicates that component B is likely to be the source core.

3C 286 (*Fig. 17*): The faint secondary component located 2.6″ west, visible in both the 1.5 and 8.4 GHz maps, and the one 0.″8 east, visible only in the 8.4 GHz map, were previously also seen by Spencer et al. (1989). A jet leads to the W component (Hines et al. 1989).

3C 298 (*Figs. 18a, b*): Our 15 and 22.5 GHz data clearly show that the core is component B1 (see also Nan Rendong et al. 1991). Components C1 and C2 are $\sim(10\pm3)\%$ polarized. About 240 mJy is missing in the 15 GHz map.

3C 299 (*Fig. 19*): This source has a secondary component at 12″ to the SW which has 5% of the flux density of the main component. Both components are clearly extended along the source major axis (Fig. 4). Observations at 8.4 GHz (van Breugel et al., in preparation) show a faint, compact core 2″ SW of the brightest component. Thus the source is a very asymmetric double with the brightest lobe being the CSS component. At 15 GHz this bright lobe is ~10–$15\%\pm2\%$ polarized.

3C 303.1 (*Fig. 20*): This source is also a very unequal double (Pearson et al. 1985). The SE component is ~5–$8\%\pm2\%$ polarized at 15 GHz. At 22.5 GHz only this component is detected.

3C 305.1: At 15 GHz (Fig. 21a) all components are polarized: $(28\pm5)\%$ (A), $(60\pm20)\%$ (B), $(22\pm4)\%$ (C) and $(7\pm3)\%$ (D). Were it not for its (marginally significant) polarization, component B would be a good candidate for the radio core, since it is the most compact and is not visible at 5 GHz (Akujor et al. 1991). The 8.4 GHz map (Fig. 21b) is very similar to that of Spencer et al. 1989 at 1.7 GHz.

3C 309.1: Comparison with single dish measurements shows that ~800 mJy are missing from our 1.5 GHz map (not shown).

3C 318 (*Fig. 22a, b*): The source is a triple (Spencer et al. 1991) with the weaker component located to the north. This component is not detected in our 15 GHz observations. Component B is $(17\pm3)\%$ polarized at the peak, component A is <9% polarized. At 22.5 GHz we detect only component B.

3C 343.1 (*Figs. 23a, b*): The source is not polarized at 15 GHz (<2% in each component).

3C 346: This source shows considerable structure. At 1.5 GHz (Fig. 5) a core and a very bright one-sided jet are embedded in a halo (possible double lobed) of $\sim14''\times12''$, accounting for $\sim60\%$

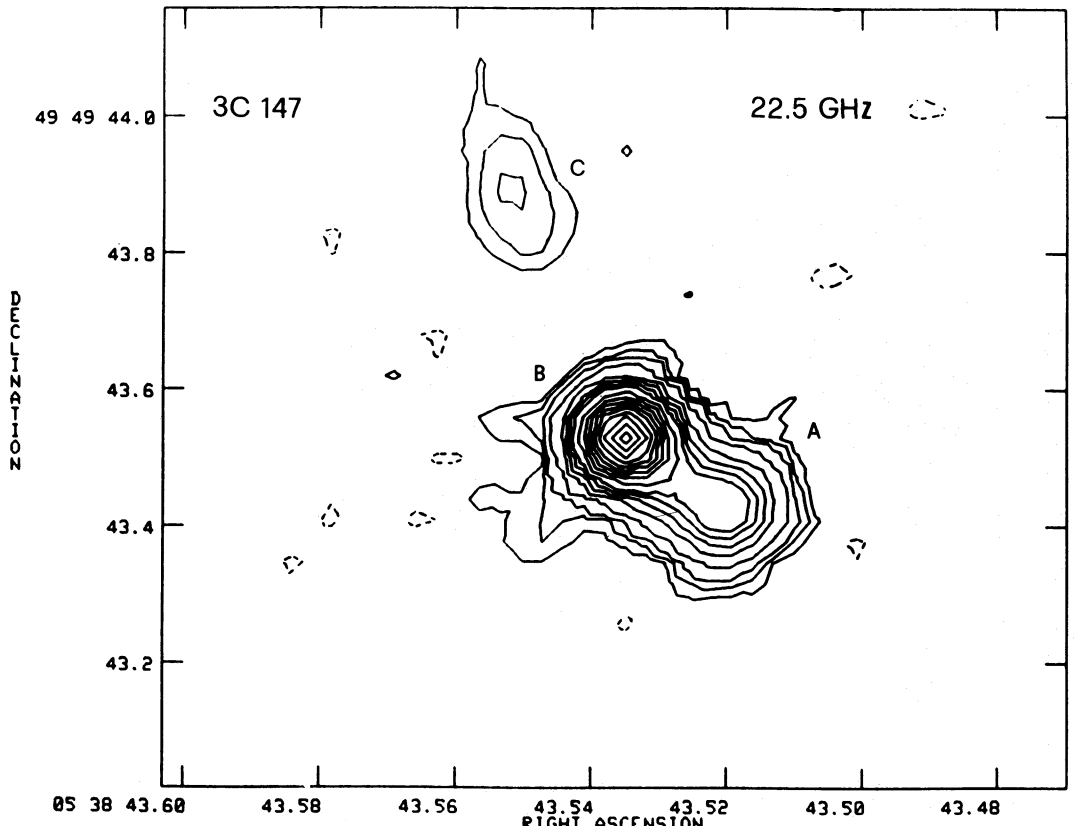

Fig. 12

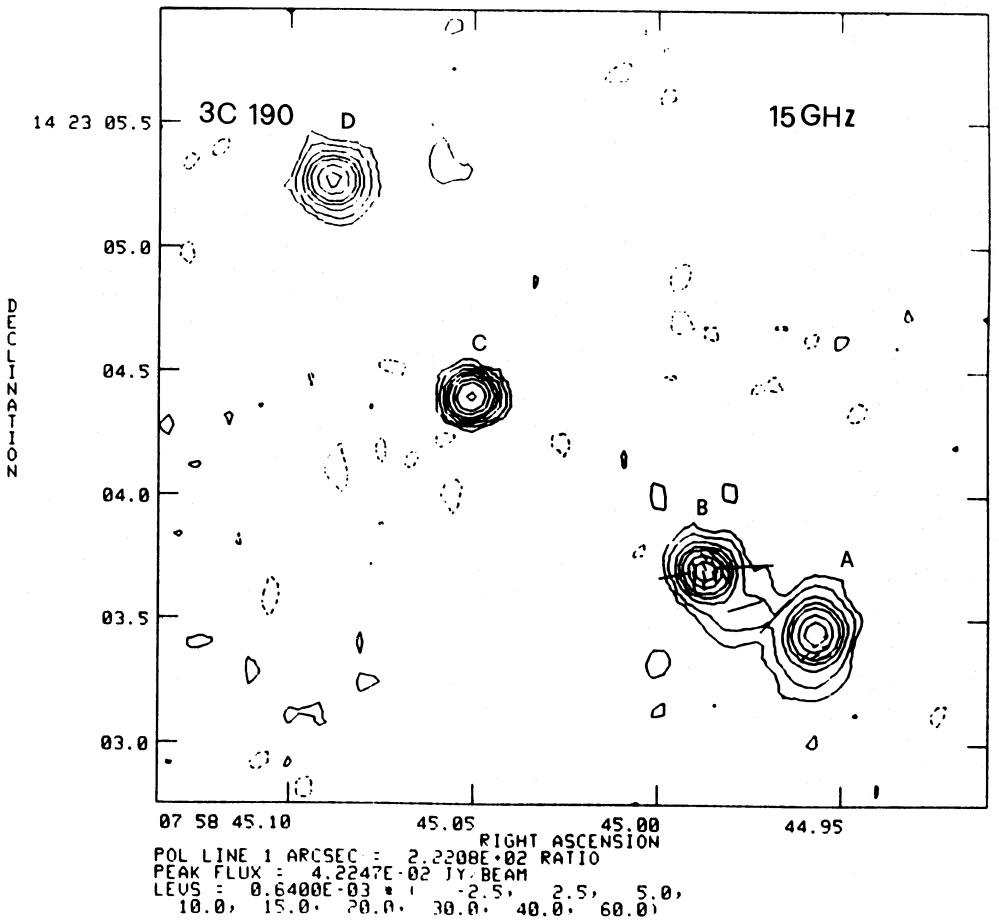

Fig. 13

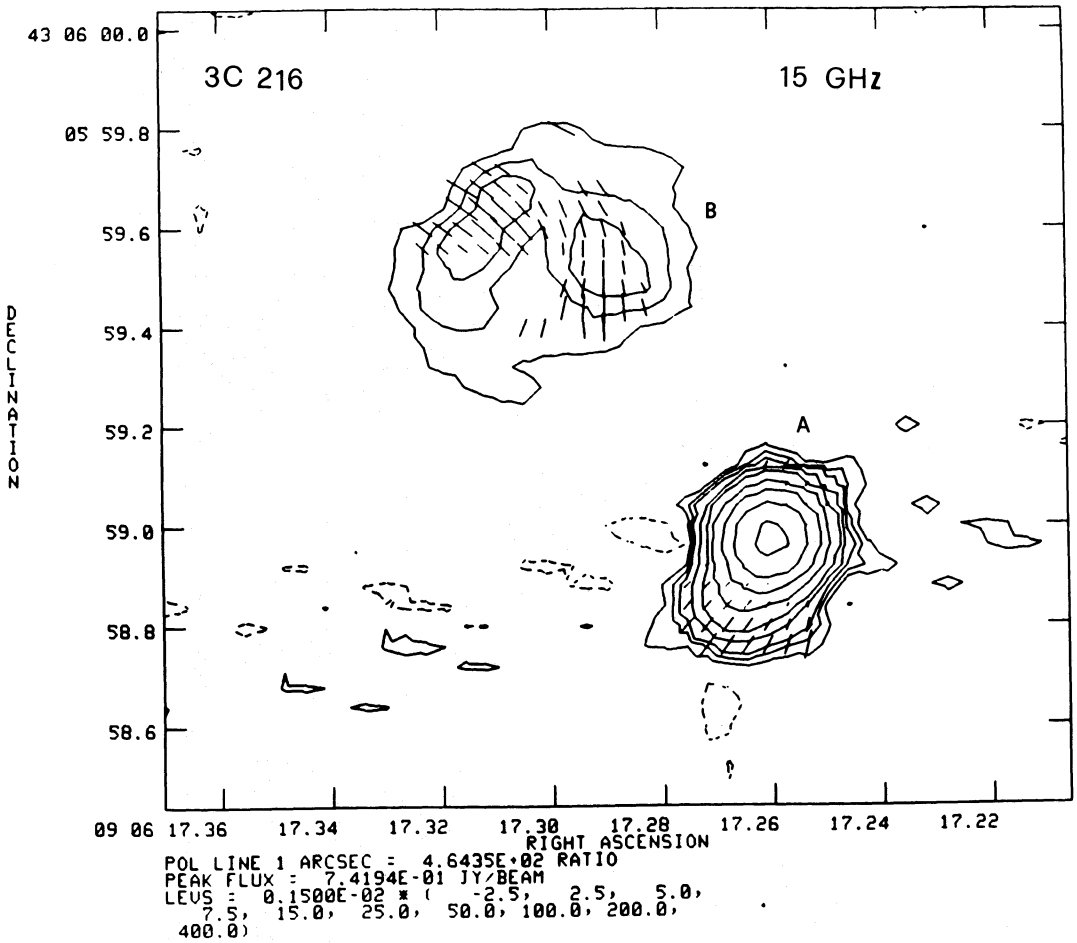

Fig. 14

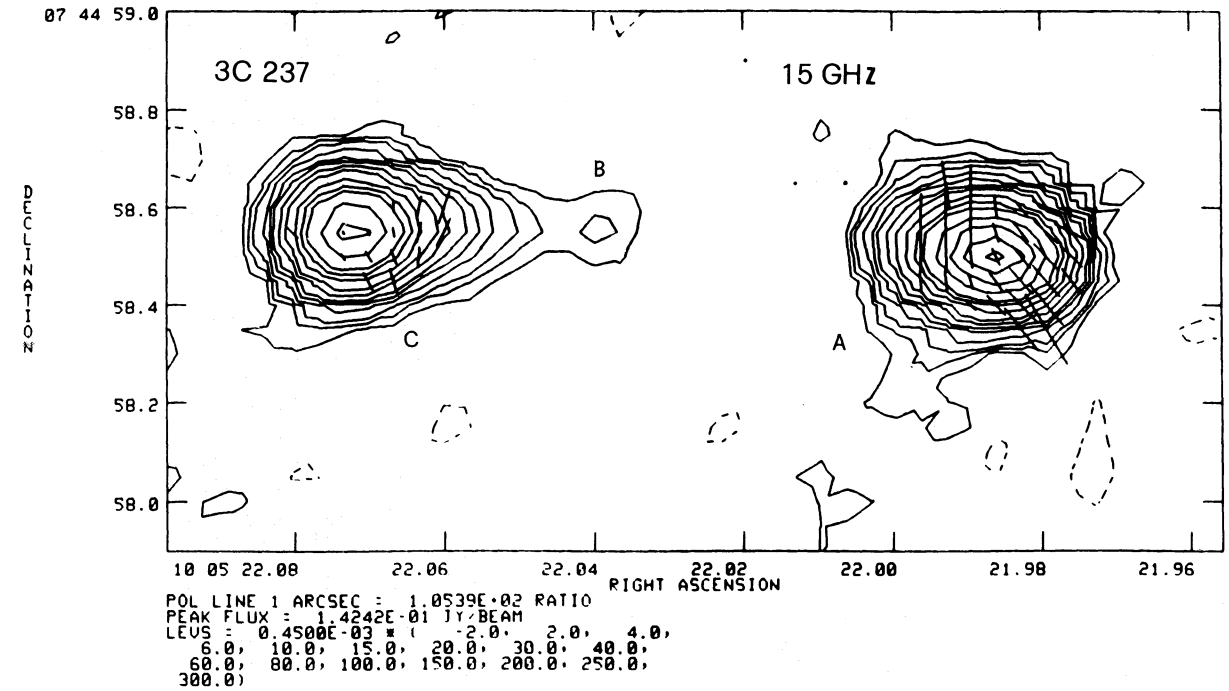

Fig. 15

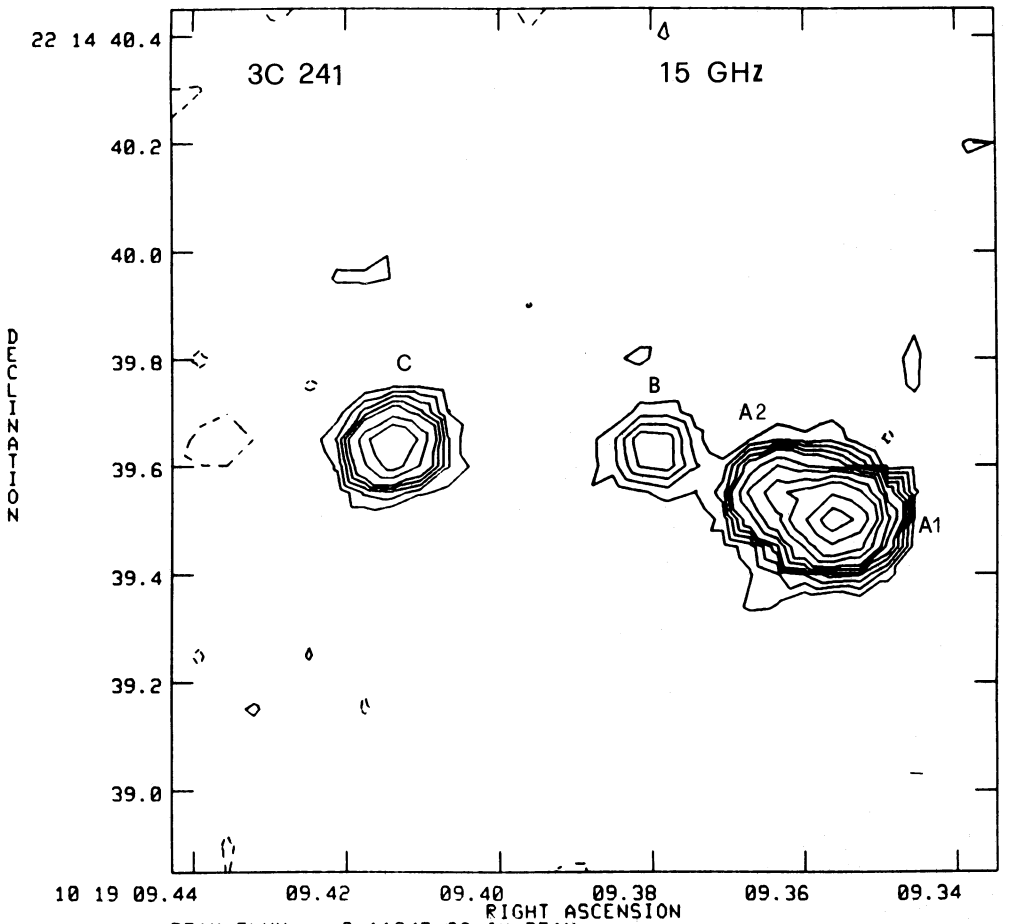

Fig. 16

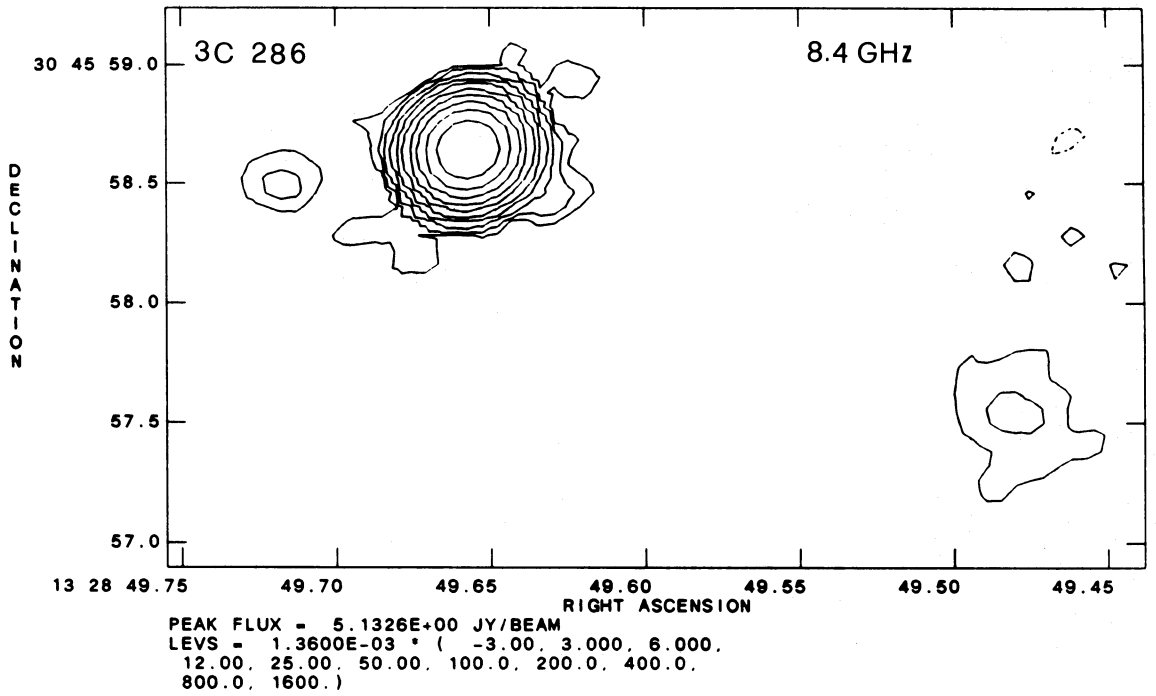

Fig. 17

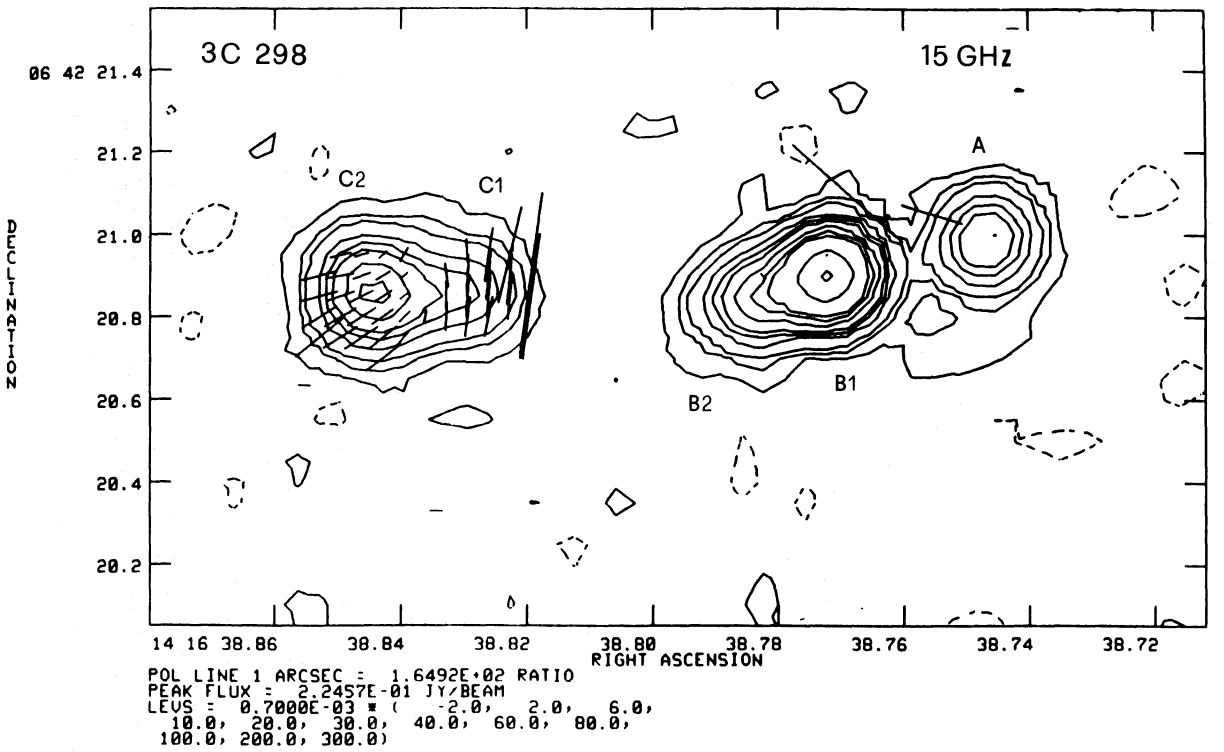

Fig. 18a

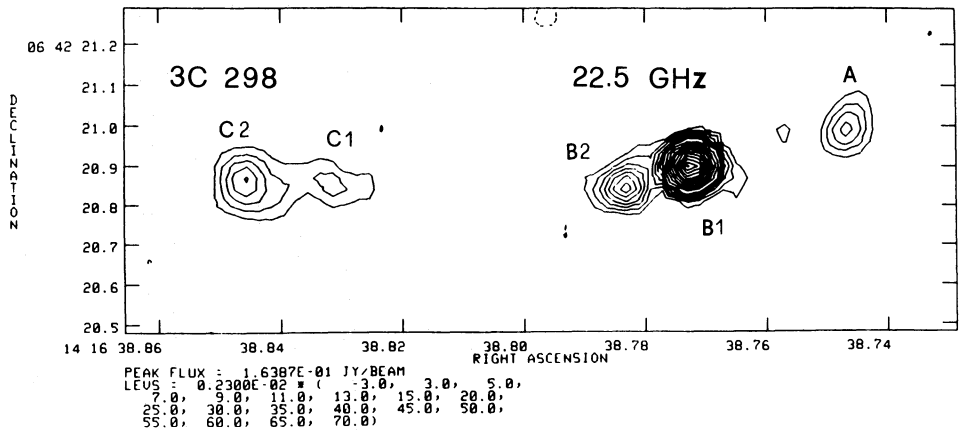

Fig. 18b

of total flux density (see also Spencer et al. 1991). At 15 GHz (Fig. 24) we do not see the halo (about 365 mJy are missing in our map), and detect only the flat spectrum core and knots in the jet. The core (A) and knots B and E are not polarized, at levels less than 2%, 16% and 20%. Knots C and D are polarized at levels of 21% and 16%.

3C 380 (*Fig. 6*): This source is surrounded by a halo of $\sim 14'' \times 9''$, accounting for $\sim 50\%$ of total flux density at 1.5 GHz. For a detailed discussion of the source structure see Wilkinson et al. (1990), and Wilkinson et al. (1991).

6. Conclusions

Observations with the VLA at 1.5, 15 and 22.5 GHz of 26 compact steep-spectrum sources (CSSs) from the 3 CR catalogue have shown the following:

(1) Only four sources, 3C 216, 3C 299, 3C 346, 3C 380, have extended emission on the scale of several arcsec. 3C 299 is found to be an asymmetric extended double and should not be classed as a CSS source. The other extended sources are consistent with the extended emission being due to the radio lobes seen in projection and overlapping with cores and jets. The remaining

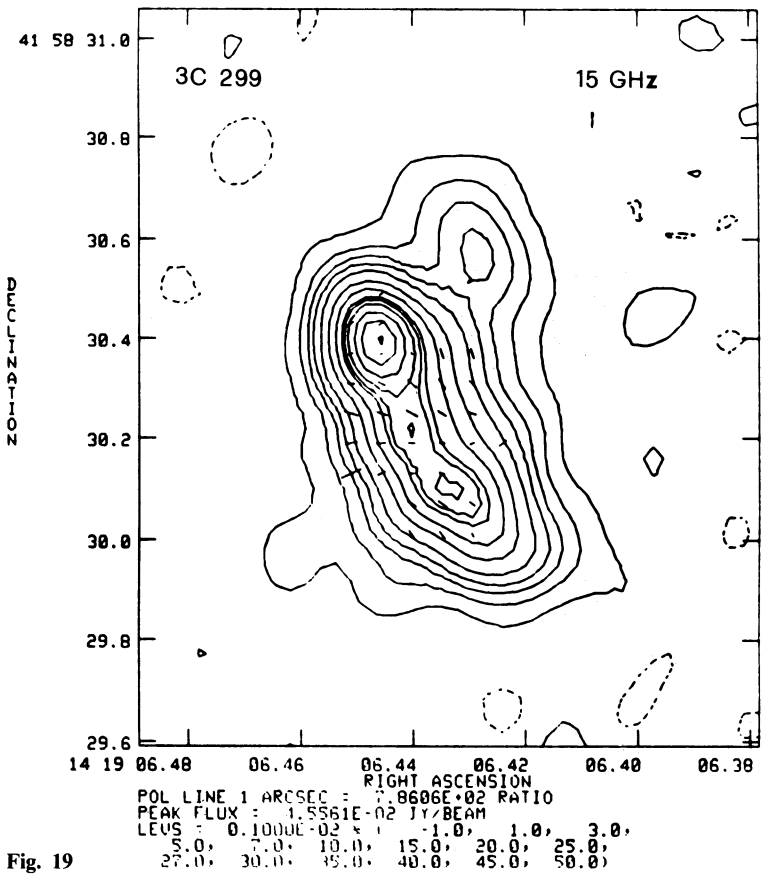

Fig. 19

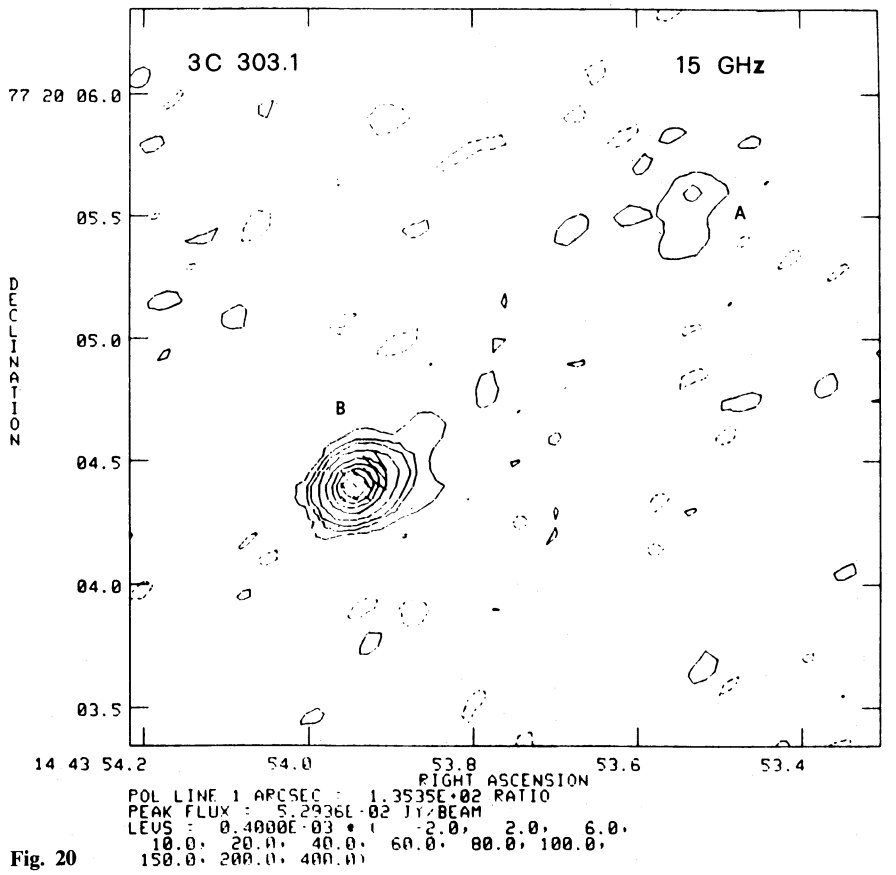

Fig. 20

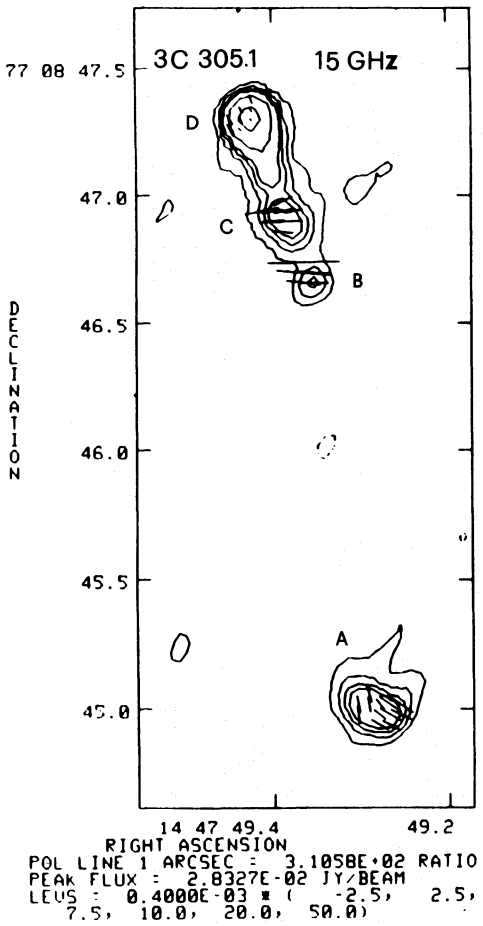

Fig. 21a

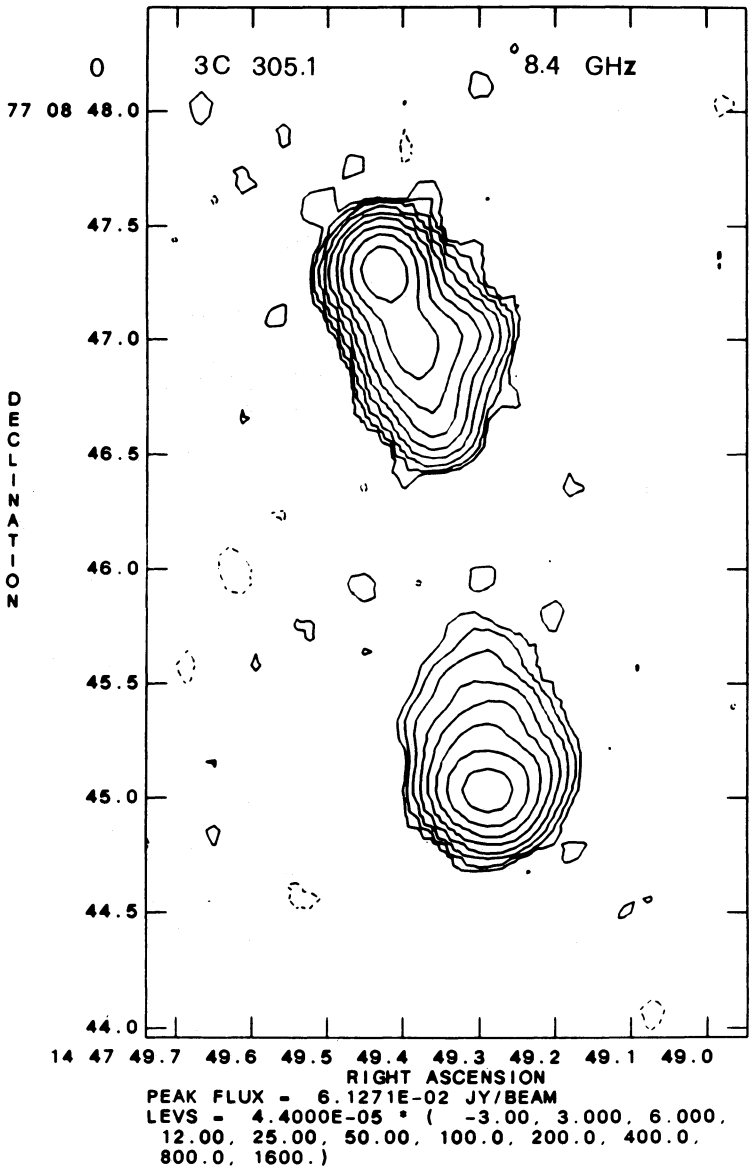

Fig. 21b

compact sources have $<3\%$ of their total luminosity in extended halo emission.

(2) Seven further sources in the sample were found to have weak compact radio cores, of which we measured the position. Cores remain still undetected in a further 9 sources.

(3) The present observations complete the radio polarization measurements at cm wavelengths on the 3 CR CSS sources (except for 3C 186). The median polarization of components at 15 GHz is $\sim 7\%$, with magnetic field direction mostly parallel to the component elongation.

Further more sensitive observations at 8.4 GHz are required to find the remaining cores. High resolution polarization measurements at 1.7 GHz should enable the level of depolarization in the sources to be found and hence an indication of the amount of gas present.

Acknowledgements. We thank R. Primavera for the photographic reproduction of the figures. The National Radio Inc., under contract with the National Science Foundation.

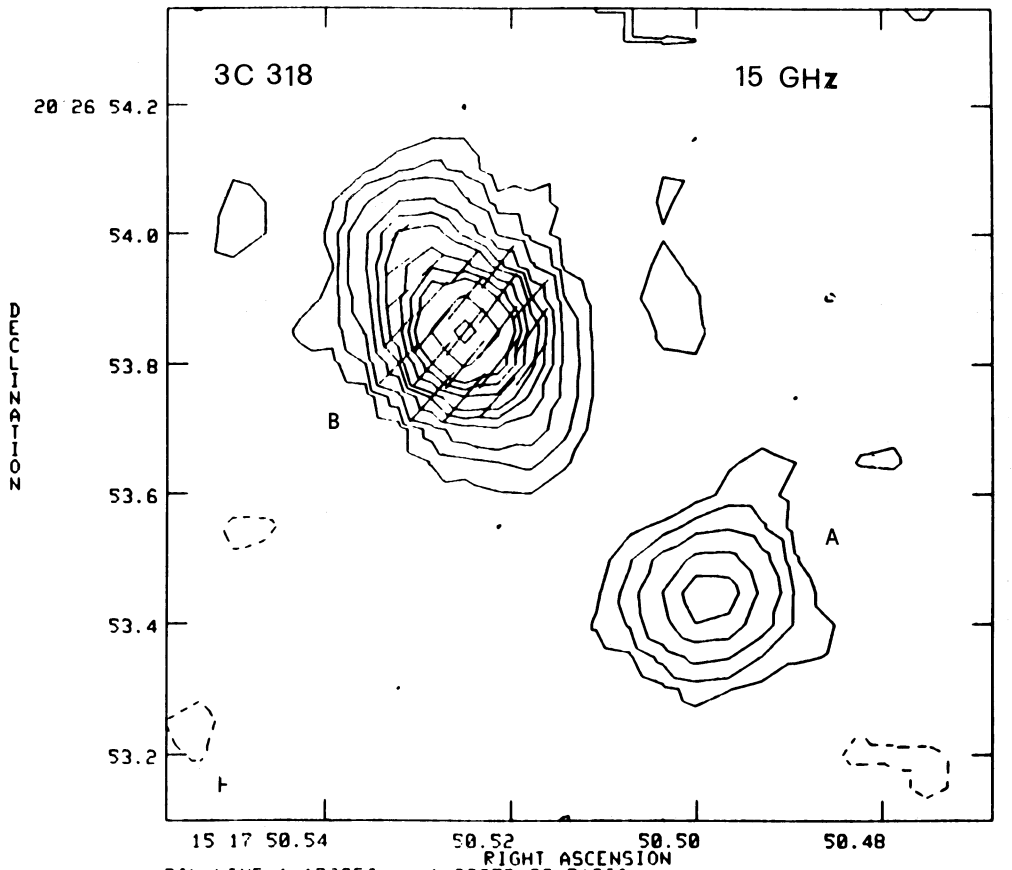

Fig. 22a

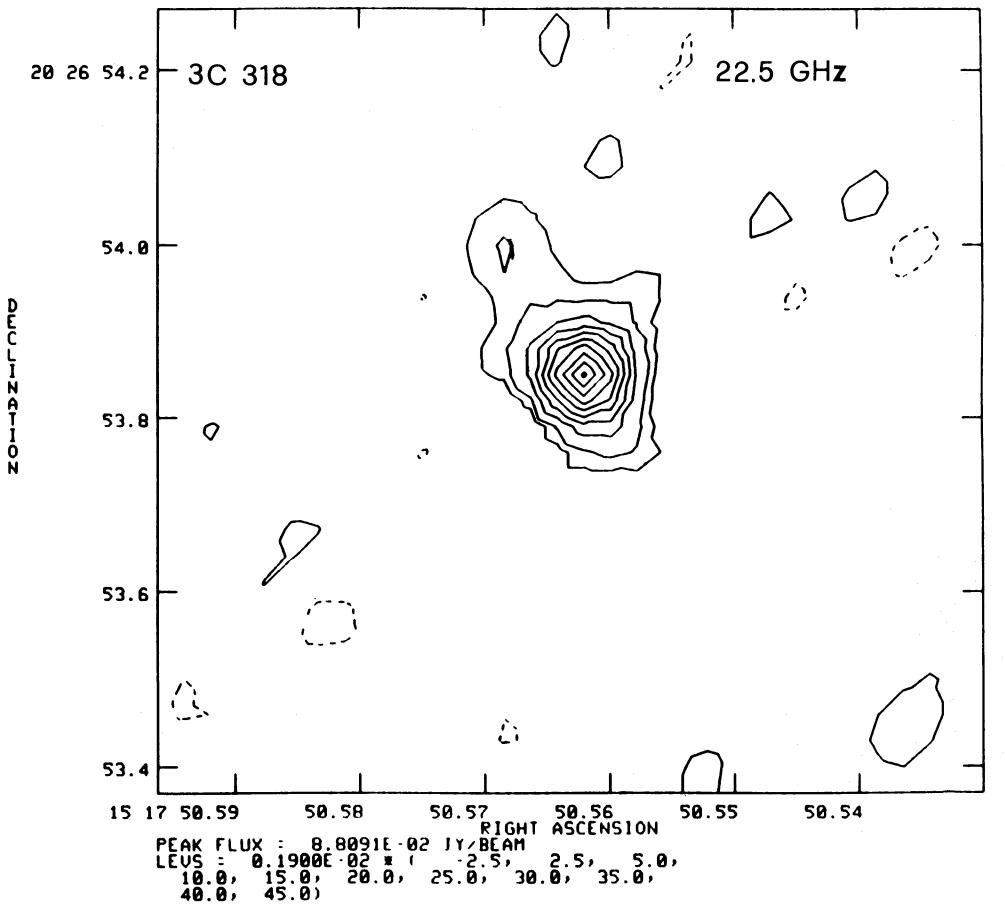

Fig. 22b

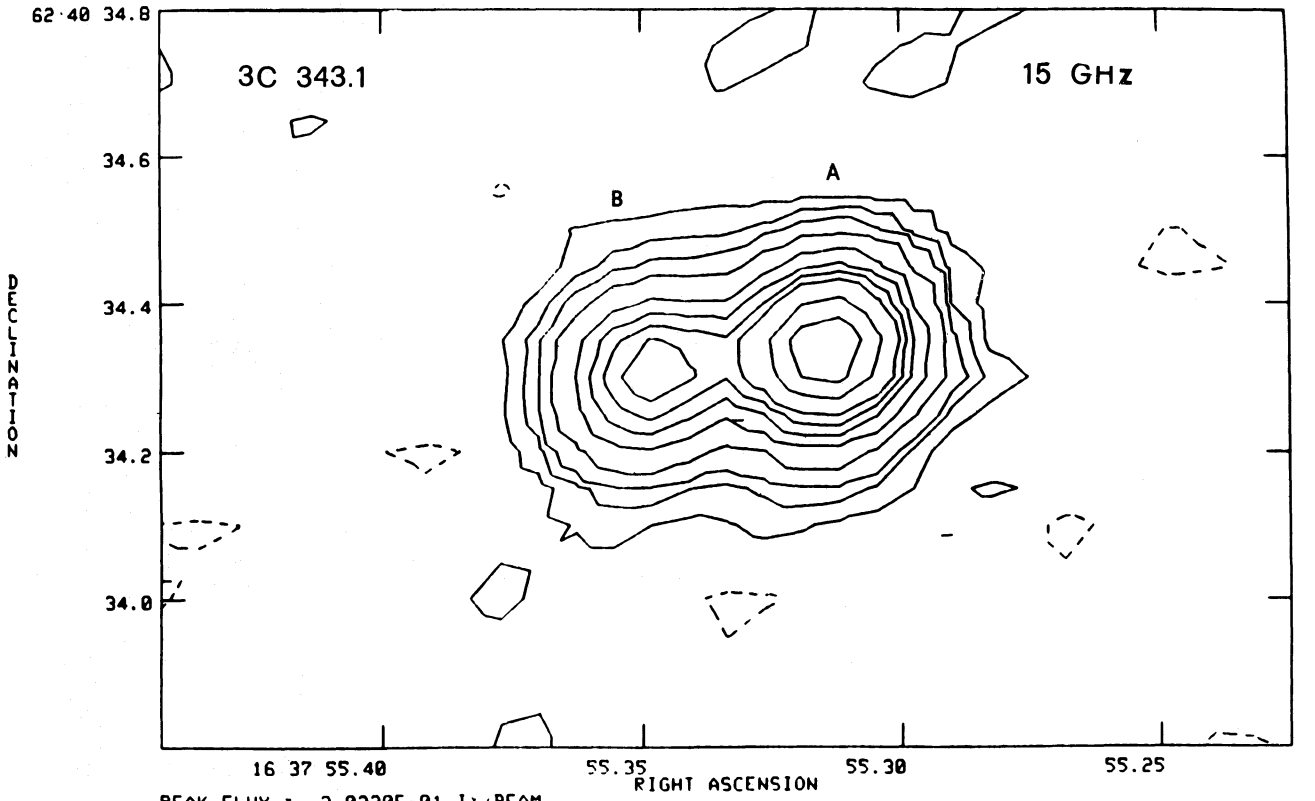

Fig. 23a

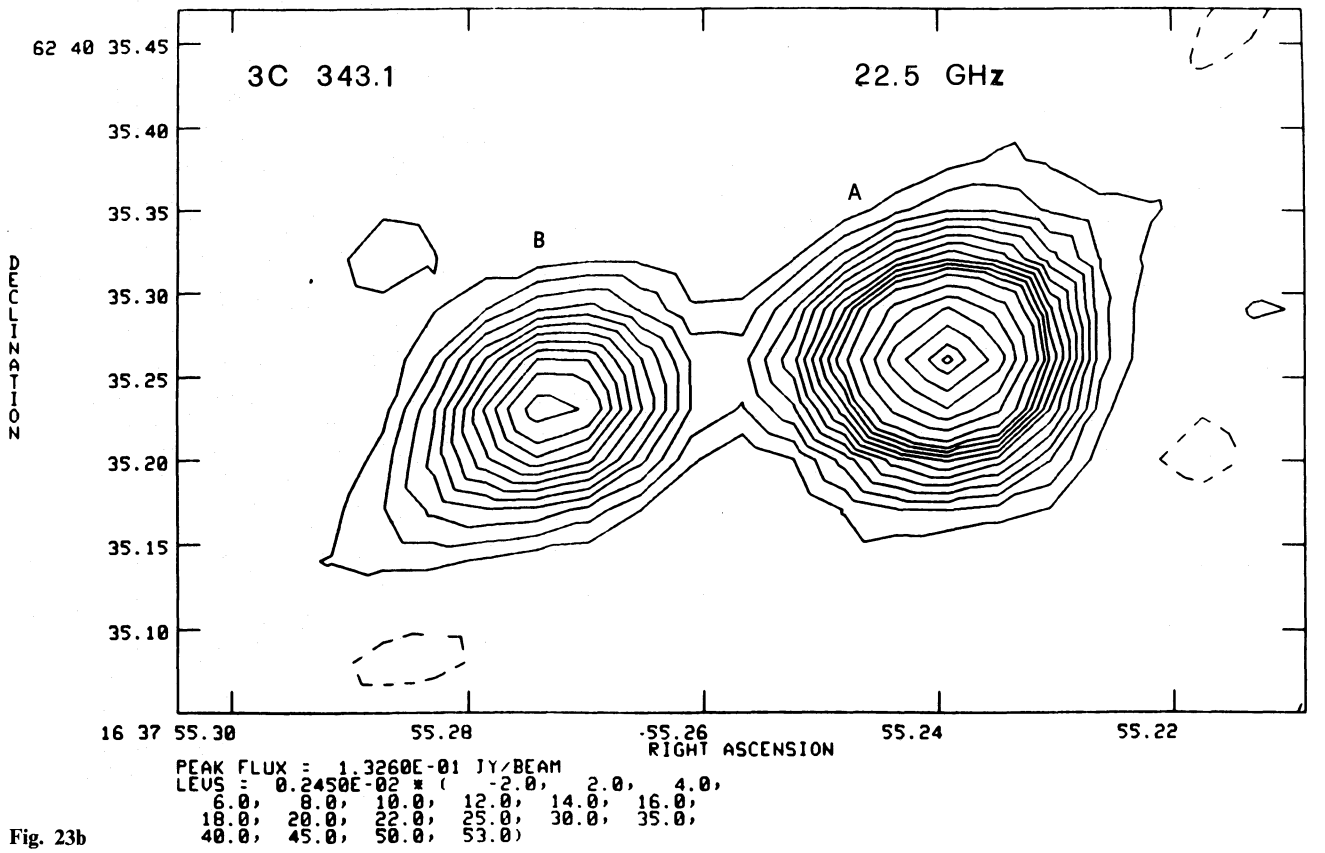

Fig. 23b

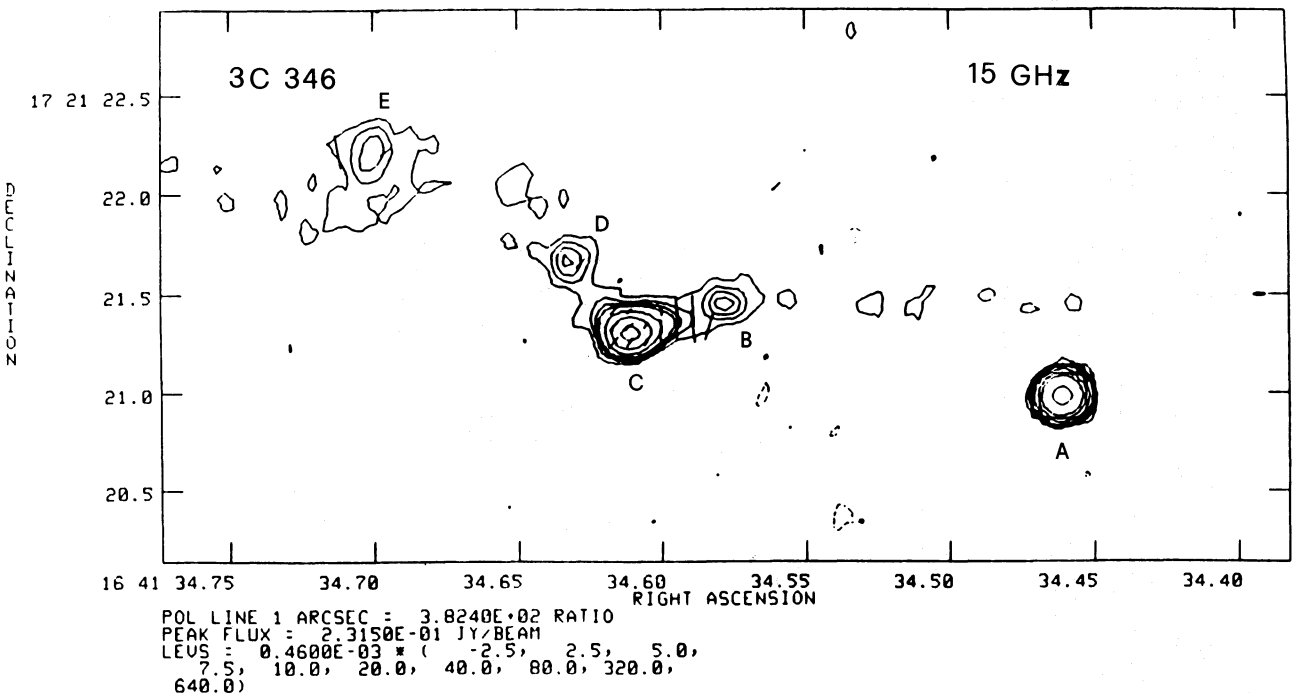

Fig. 24

References

Akujor C.E., Spencer R.E., Wilkinson P.N., 1990, MNRAS 244, 362

Akujor C.E., Spencer R.E., Zhang F.J., et al., 1991a, MNRAS 250, 215

Akujor C.E., Spencer R.E., Saikia D.J., 1991b, A&A (in press)

Akujor C.E., Spencer R.E., Wilkinson P.N., 1991c, MNRAS (in press)

Barthel P.D., Pearson T.J., Readhead A.C.S., 1988, ApJ 329, L51

Bridle A.H., Fomalont E.B., Cornwell T.J., 1981, AJ 86, 1294

Cawthorne T.V., Scheuer P.A.G., Morison I., Muxlow T.W.B., 1986, MNRAS 219, 883

de Ruiter H.R., Parma P., Fanti C., Fanti R., 1990, A&A 227, 351

De Waard, 1984, Ph.D. Thesis, Leiden University

Fanti C., Fanti R., Parma P., Schilizzi R.T., van Breugel W.J.M., 1985, A&A 143, 292

Fanti C., Fanti R., Parma P., et al., 1989, A&A 217, 44

Fanti R., Fanti C., Schilizzi R.T., et al., 1990, A&A 231, 333

Hines D.C., Owen F.N., Eilek J.A., 1989, ApJ 347, 713

Kuhr H., Witzel A., Pauliny-Toth I.I.K., Nauber U., 1981, A&AS 45, 367

Nan Rendong, Schilizzi R.T., Fanti C., Fanti R., 1991, A&A 245, 449

Pearson T.J., Perley R.A., Readhead A.C.S., 1985, AJ 90, 738

Perley R.A., 1989, in: Proc. Workshop on Hot Spots in Extragalactic Radio Sources. Meisenheimer and Roser (eds.) Springer, Berlin, p. 1

Riley J.M., Pooley G.G., 1975, Mem. R. Astron. Soc. 80, 105

Saikia D.J., Singal A.K., Cornwell T.J., 1987, MNRAS 224, 379

Schilizzi R.T., Kapahi V.K., Neff S.G., 1982, J. Astrophys. Astron. 3, 173

Schilizzi R.T., Skillman E.D., Miley G.K., et al., 1988, in: Reid M.J., Moran J.M. (eds.) IAU Symp. 129, The Impact of VLBI on Astrophysics and Geophysics. Kluwer, Dordrecht, p. 127

Simon R.S., Readhead A.C.S., Moffet A.T., et al., 1990, ApJ 354, 140

Spangler S., 1982, VLA Scientific Memorandum, N. 136

Spencer R.E., McDowell J.C., Charlesworth M., et al., 1989, MNRAS 240, 657

Spencer R.E., Schilizzi R.T., Fanti C., et al., 1991, MNRAS 250, 255

Spinrad H., Djorgoski S., Marr J., Aguilar L., 1985, Publs. Ast. Soc. Pac. 97, 932

van Breugel W.J.M., Miley G.K., Heckman T.A., 1984, AJ 89, 5 (vBMH)

Wilkinson P.N., Tzioumis A.K., Akujor C.A., et al., 1990, in: Zensus A., Pearson T.J. (eds.) Workshop on Parsec Scale Radio Jets. Camb. Univ. Press, Cambridge, p. 152

Wilkinson P.N., Akujor C.A., Cornwell T.J., Saikia D.J., 1991, MNRAS 248, 86

Windhorst R., 1984, Ph.D. Thesis, Leiden University